# Rockwall slope erosion in the NW Himalaya

**Elizabeth N. Orr[1,2*], Lewis A. Owen[3], Sourav Saha[4], Sarah J. Hammer[5], Marc W. Caffee[6,7]**

[1] *GFZ German Research Centre for Geosciences, Telegrafenberg, 14473 Potsdam, Germany*
[2] *Institute for Geosciences, University of Potsdam, 14476 Potsdam, Germany*
[3] *Department of Marine, Earth, and Atmospheric Sciences, North Carolina State University, Raleigh, NC 27695, USA*
[4] *Department of Earth, Planetary, and Space Sciences, University of California, Los Angeles, CA 90095, USA*
[5] *Department of Geology, University of Cincinnati, Cincinnati, OH 45221, USA*
[6] *Department of Physics, Purdue University, West Lafayette, IN 47907, USA*
[7] *Department of Earth, Atmospheric and Planetary Sciences, Purdue University, West Lafayette, IN 47907, USA*

*Corresponding author: Elizabeth N. Orr (elizabeth.orr@gfz-potsdam.de)

---

**Key Points:**

- Rates of periglacial rockwall slope erosion are defined for the NW Himalaya using cosmogenic $^{10}$Be concentrations in sediment from medial moraines.

- Beryllium-10 concentrations range from 0.5±0.04x$10^4$ to 260.0±12.5x$10^4$ at/g, which yield erosion rates between 0.02±0.04 and 7.6±1.0 mm/a.

- Tectonically driven uplift is a first order control on patterns of slope erosion in the NW Himalaya. Precipitation likely plays a secondary role.

**Abstract**

Steep north-south trending gradients in elevation, slope, relief, rock uplift and precipitation make the NW Himalaya an excellent location to examine the relative roles of climate and tectonics in erosion and landscape evolution. We define the distribution and magnitude of periglacial rockwall slope erosion across 12 catchments in Himachal Pradesh and Jammu and Kashmir in the Himalaya of northern India using cosmogenic $^{10}Be$ concentrations in sediment from medial moraines. Beryllium-10 concentrations range from $0.5\pm0.04\times10^4$ to $260.0\pm12.5\times10^4$ at/g, which yield erosion rates between $0.02\pm0.04$ and $7.6\pm1.0$ mm/a. Between ~0.02 and ~8 m of rockwall slope erosion would be possible in this setting across a single millennium, and >2 km when extrapolated for the Quaternary period. This erosion affects catchment sediment flux and glacier dynamics, and helps to establish the pace of topographic change at the headwaters of catchments. We combine rockwall erosion records from the Himalaya of Himachal Pradesh, Jammu and Kashmir and Uttarakhand in India and Baltistan in Pakistan to create a regional erosion dataset. Rockwall slope erosion rates progressively decrease with distance north from the Main Central Thrust and into the interior of the orogen. The distribution and magnitude of this erosion is most closely associated with records of Himalayan denudation and rock uplift, where the highest rates of change are recorded in the Greater Himalaya sequences. This suggests that tectonically driven uplift, rather than climate, is a first order control on patterns of slope erosion in the NW Himalaya. Precipitation would therefore come as a secondary control.

**Keywords:** periglacial erosion; rock uplift; climate; cosmogenic isotopes; sediment flux

## 1. Introduction

A number of studies have underlined the importance of periglacial rockwall slope erosion in high altitude mountain settings, and its role in catchment sediment flux, relief production, topographic configuration and glacier dynamics (Heimsath and McGlynn, 2008; MacGregor et al., 2009; Seong et al., 2009; Ward and Anderson, 2011; Benn et al., 2012 Scherler and Egholm, 2017; Orr et al., 2019). The lateral erosion of slopes has been shown to exceed rates of vertical incision through glacial and fluvial processes, and therefore to a greater extent than previously thought, contribute to denudation budgets and landscape change on the catchment and mountain range scale (Brocklehurst and Whipple, 2006; Foster et al., 2008).

Steep north-south gradients in elevation, slope, relief, rock uplift and precipitation has made the Himalayan-Tibetan orogen an ideal location to evaluate landscape evolution controls (Bookhagen and Burbank, 2006, 2010; Scherler et al., 2011). Short and long-term erosion in the orogen has been shown to scale with tectonics (Burbank et al., 2003; Scherler et al., 2014; Godard et al., 2014), rainfall (Thiede et al., 2004; Grujic et al., 2006; Clift et al., 2008; Gabet et al. 2008; Wulf et al., 2010; Deeken et al., 2011) and/or topography (Vance et al., 2003; Scherler et al., 2011, 2014). Which of these parameters, if any, provide a first-order control on rates of rockwall slope erosion remains unclear.

Orr et al. (2019) was able to identify a tentative relationship between rockwall slope erosion and precipitation in the NW Himalaya. Higher rates of erosion, for example, were determined for catchments with enhanced monsoon precipitation. Rather than identifying a single control, their study instead suggests that rockwall slope erosion is more complex, and is dictated by the interaction between tectonics, climate, topography, and surface processes that are specific to each catchment. This opposes the view that in tectonically active mountain ranges, the strength of hillslope-glacier coupling is largely controlled by rock uplift and topographic steepness (Scherler et al., 2011; Gibson et al., 2017).

In this study, we seek to better define the distribution and magnitude of rockwall slope erosion in the NW Himalaya by building upon the work of Orr et al. (2019) and quantifying erosion rates for a suite of 12 catchments. Rates of rockwall slope erosion are derived from terrestrial cosmogenic nuclide (TCN) $^{10}$Be concentrations measured in sediment from medial moraines. Our new erosion dataset is combined with existing slope erosion records from Seong et al. (2009), Scherler and Egholm (2017) and Orr et al. (2019). This regional rockwall erosion dataset is compared to records of catchment-wide erosion and exhumation for the NW Himalaya to evaluate the extent to which slope erosion may differ from other records of landscape change, which have been averaged across various spatial and temporal scales. We compare patterns of slope erosion to variations in geology, tectonics, climate and topography throughout the region, to resolve the primary controls of rockwall slope erosion in the NW Himalaya. Finally, we determine to what extent slope erosion and its controls, in this high-altitude and high relief setting, can contribute to the longstanding debate over the significance of climate versus tectonics in driving both short and long term landscape change.

## 2. Regional Setting

The Himalayan-Tibetan orogen has formed as the result of the continued continental collision and partial subduction between the Indian and Eurasian lithospheric plates (Searle et al., 1997). The Indus-Tsangpo Suture Zone (ITSZ) defines the collision zone between these plates in the NW Himalaya and contains remnants of the Neo-Tethys Ocean (Fig. 1). The suture zone marks the northern boundary of the Tethyan Himalaya (Searle, 1986; Steck et al., 1998; Schlup et al., 2003). Between the early Miocene and Pleistocene, deformation driven crustal shortening initiated the development of a sequence of foreland propagating thrust systems that divide the lithotectonic units that lie south of the Tethyan Himalaya. The South-Tibetan Detachment (STD) and the Main Central Thrust (MCT) bound the Greater Himalaya Crystalline Core Zone to the north and south, respectively (Frank et al., 1973; Searle and Fryer, 1986; Walker et al., 1999; Miller et al., 2001; Vannay et al., 2004). This unit has been divided into two sub-units: southern Greater Himalaya sequence (GHS-S) and northern Greater Himalaya sequence (GHS-N; DeCelles et al., 2001; Thiede and Ehlers 2013). South of the Greater Himalaya and MCT lies the Lesser Himalaya sequence which is bounded to the south by the Main Boundary Thrust (MBT). South of the MBT lies the Sub-Himalaya and Main Frontal Thrust (MFT; Upreti, 1999; Miller et al., 2000; Vannay et al., 2004).

Continued crustal shortening and thrust and strike-slip faulting throughout the orogen means that the NW Himalaya remains tectonically active (Hodges et al., 2004; Vannay et al., 2004; Bojar et al., 2005), even though some regions in northern India such as Ladakh, have undergone tectonic quiescence or dormancy since the early Miocene (Kristein et al., 2006, 2009). Hodges (2000), Yin and Harrison (2000) and Streule et al. (2009) provide further details of the Himalayan lithotectonic units and the timing of movement throughout the fault systems.

Two atmospheric systems primarily govern northwest Himalayan climate: the Indian summer monsoon that advects moisture from the Indian Ocean between late May and September, and the Northern Hemispheric mid-latitude westerlies, which bring moisture from the Mediterranean, Black and Caspian seas between December and March (Gadgil 2003; Lang and Barros 2004; Wulf et al., 2010; Mölg et al., 2013). A steep south-north precipitation gradient became established during the late Miocene, perpendicular to the strike of the mountain belt (~8 Ma; Qiang et al., 2001; Liu and Dong, 2013), due to the high elevation ranges of the Greater Himalaya inhibiting the northward migration of moisture to the interior of the orogen. Monsoon air masses are forced to ascend, condense and form clouds along the Himalayan front, which creates a rainshadow down the leeside of this orographic barrier (Bookhagen et al., 2005a, b; Wulf et al., 2010). During times of increased monsoon strength, moisture is thought to penetrate farther into the interior of the orogen (Finkel et al., 2003 Bookhagen et al., 2005a, b; Wulf et al., 2010). The northern hemispheric mid-latitude westerlies operate at higher tropospheric levels to the Indian summer monsoon. The orographic capture of moisture transported by this atmospheric system is therefore focused in high elevation ranges (> 4500 m asl) as winter snowfall (Weiers 1995; Lang and Barros 2004). Today, mean annual precipitation declines from ~1500−3000 mm in the Lesser and Greater Himalaya ranges, to <150 mm in the interior of the Tethyan Himlaya and Tibetan Plateau (Bookhagen and Burbank, 2006).

The distribution and magnitude of precipitation has been shown to vary both temporally and spatially throughout the Himalayan-Tibetan orogen during the late Quaternary (Burbank et al., 2003; Bookhagen et al., 2005a, b). Fluctuations in monsoon strength driven by changes in orbital insolation, the migration of the intertropical convergence zone, convective localized monsoon storms and sporadic heavy rainfall are thought to cause some of this variability (Finkel et al., 2003; Owen et al., 2008; Thomas et al., 2016). On the local to regional scale ($10^{2-4}$ km$^{2}$), topography and wind direction exert controls on the migration of moisture throughout the NW Himalaya (Bookhagen et al., 2005a, b), and create localized microclimates throughout individual mountain ranges (Benn and Owen, 1998; Bookhagen and Burbank, 2010; Wulf et al., 2010). Landscape change in the NW Himalaya is precipitation sensitive, where shifts in the availability and source of moisture has been shown to initiate changes to sediment flux, hillslope processes (Bookhagen et al., 2005; Bookhagen and Burbank, 2006; Sharma et al., 2017; Kumar et al., 2018) and the timing of glaciation (Owen and Dortch, 2014; Saha et al., 2018).

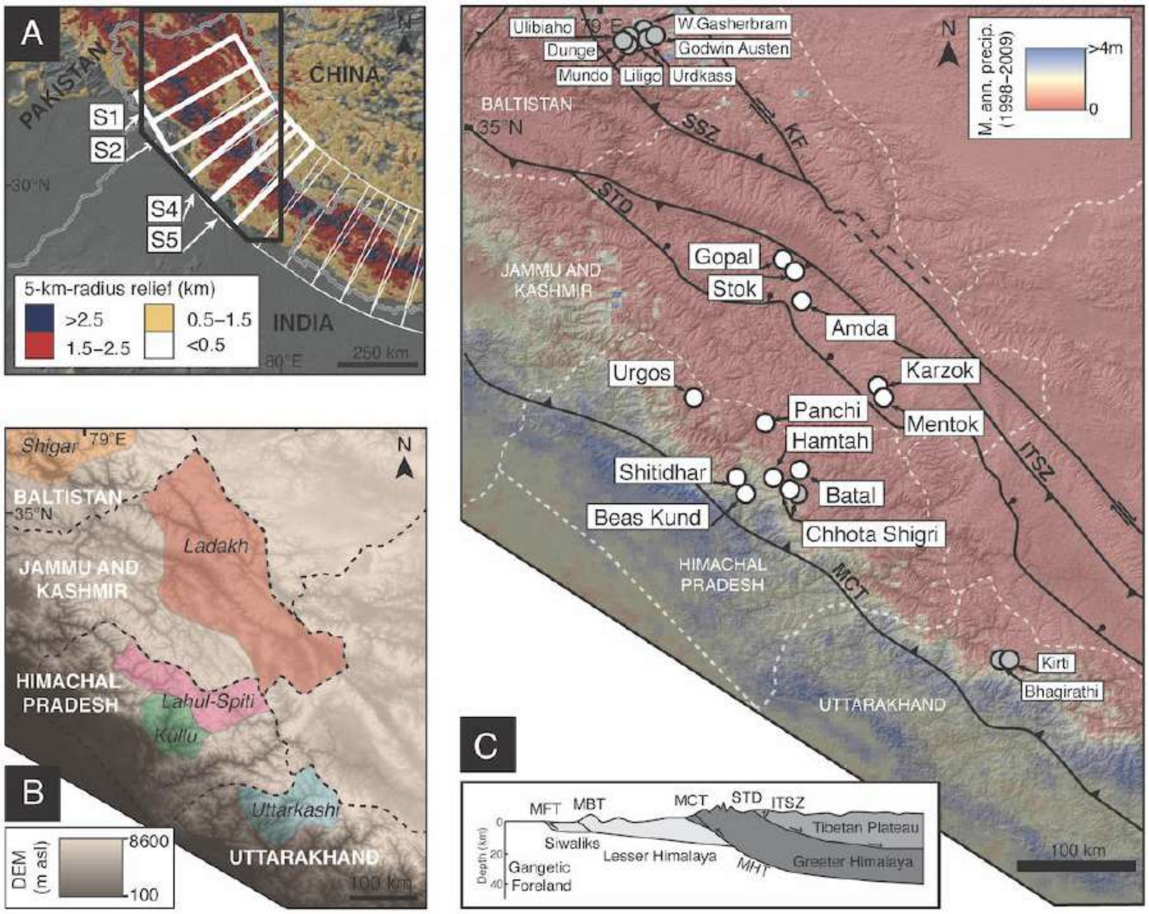


**Fig. 1.** Overview of the study area in the NW Himalaya. a) Study area location (black polygon) is outlined on a 5-km-radius relief map with swath polygons [bold polygons S1, 2, 4, 5 are referred to in Fig. 7] modified from Bookhagen and Burbank (2006). 3-km-radius relief dataset used in following analyses. b) ASTER GDEM of study area (see a) with investigated regions and districts outlined. c) Hillshade map of the study area is overlain by mean annual precipitation (TRMM 2B31; Bookhagen and Burbank, 2006). White circles: location of investigated catchments of this study. Gray circles: location of published rockwall slope erosion rate studies (Seong et al., 2009; Scherler and Egholm 2017; Orr et al., 2019). Major faults from Hodges (2000) and Schlup et al. (2003). KF- Karakoram Fault, SSZ- Shyok Suture Zone, ITSZ - Indus-Tsangpo Suture Zone STD- South Tibetan Detachment, MCT- Main Central Thrust, MBT- Main Boundary Thrust, MFT- Main Frontal Thrust, MHT- Main Himalayan Thrust. Inset: simplified structure of the NW Himalaya, modified from Searle et al. (2011) and Schlup et al. (2011).

The timing and forcing of glaciation can also vary across short distances ($10^{1-2}$ km) in the NW Himalaya (Owen and Dortch 2014). Studies have shown that the nature of glaciation can be influenced by climatic factors such as shifts in the strength or behavior of regional and/or global atmospheric and oceanic systems (Owen and Sharma 1998; Watanabe et al., 1998; Solomina et al., 2015; 2016; Saha et al., 2018) and/or local geological factors such as topography and glacier type (Barr and Lovell 2014; Anderson et al., 2014). The Himalayan Holocene stages (HHs; Saha et al., 2018), Himalayan-Tibetan Holocene glacial stages (HTHS; Saha et al., 2019), semi-arid western Himalayan-Tibetan orogen stages (SWHTs; Dortch et al., 2013) and monsoonal Himalayan-Tibetan stages (MOHITs; Murari et al., 2014) provide regional syntheses of the glacial records throughout the NW Himalaya (Table 1).

### *2.1. Study Areas*

We selected 12 accessible catchments along the south-north precipitation gradient of the NW Himalaya (Figs. 1, 2, Supplementary Item 2). Each catchment supports either a cirque or small valley glacier with distinct and well-preserved medial moraines. The northern-most sites of this study are located in the Ladakh and Zanskar Ranges of the Ladakh region in Jammu and Kashmir of northern India and the Shigar region of Baltistan in Pakistan (Fig. 1). For this latter site, a pre-existing erosion dataset is reanalyzed only. The Indian summer monsoon delivers two-thirds of the annual precipitation to Ladakh (87 mm/a; Table 1), whereas the mid-latitude westerlies provide the primary source of moisture to the Shigar region. Glaciers in the Ladakh region are small (1–10 $km^2$) cold-based sub-polar glaciers, which are precipitation sensitive and sublimation dominated (Benn and Owen, 2002).

**Table 1.** Details of the investigated catchments.

The arid/semi-arid climatic setting of the Ladakh region is largely responsible for the preservation of very old landforms and sediment deposits (>400 ka; Owen et al., 2006; Hedrick et al., 2011; Orr et al., 2017, 2018) and slow rates of landscape change (<0.07±0.01 mm/a; Dortch et al., 2011a; Dietsch et al., 2015). The investigated Gopal, Stok and Amda catchments are three north-facing transverse catchments in the high-altitude desert landscapes of the northern Zanskar Range in Ladakh that retain small valley glaciers (Figs. 1, 2; Table 1). Karzok and Mentok are northeast-trending catchments that drain the Rupshu Massif in central Zanskar of the Ladakh region. Cirque glaciers occupy the upper reaches of these catchments.

The Lahul-Spiti and Kullu district catchments are located in Pir Panjal and Greater Himalaya ranges of the Himachal Pradesh in northern India. Precipitation is primarily sourced from the Indian summer monsoon (950–1020 mm/a; Table 1). Glaciers are large, temperate and melt dominated, and fed by precipitation from the summer monsoon and mid-latitude westerlies (Benn and Owen, 2002; Su and Shi, 2002). The Urgos valley glacier extends throughout the upper reaches of a southeast trending tributary catchment of the Miyar basin in the Lahul-Spiti district (Fig. 2). Panchi is a north-facing catchment with a small valley glacier, located north of the Keylong and Darcha villages. Shitidar, Batal, Chhota Shigri and Hamtah are north facing tributary catchments with one or two valley glaciers. Beas Kund is a southeast trending catchment located on the southern slopes of the Pir Panjal Range in the Kullu district. Two valley glaciers occupy this catchment.

The Indian summer monsoon also dominates annual precipitation in the Uttarkashi district of Uttarakhand, northern India, a region our study revisits and reanalyses rockwall erosion data (Orr et al., 2019).

## 3. Methodology

Geomorphic maps of the periglacial-glacial realms of the 12 investigated catchments were prepared in the field and then refined using Advanced Spaceborne Thermal Emission and Reflection Radiometer (ASTER) global digital elevation models (GDEMs; 30-m-resolution), Landsat Enhanced Thematic Mapper Plus (ETM+) imagery and Google Earth imagery. The rockwall of each catchment is defined as the headwater slopes above the equilibrium-line altitude of each glacier. Topographic and geomorphic parameters including catchment area, 3-km-radius relief, mean slope, hypsometry and aspect were calculated using the Spatial Analyst Toolbox in ArcMap 10.1. These analyses were also conducted for the Baltoro glacier system in the Shigar of Baltistan, Pakistan (Seong et al., 2009) and the Bhagirathi glacier system in the Uttarkashi district of Uttarakhand, northern India (Orr et al., 2019) to enable comparisons between rockwall slope erosion and catchment parameters throughout the NW Himalaya.

Rates of rockwall slope erosion are inferred for each catchment by measuring TCN concentrations of medial moraine sediment. Medial moraines form within the glacier ablation zones as a result of englacial debris melt out in our selected study areas. This debris is sourced and transferred from accumulation zone slopes to the glacier surface via rockfall processes and avalanching, before being transported englacially to the equilibrium line of the glacier and exhumed to the surface (Matsuoka and Sakai, 1999; Goodsell et al., 2005; MacGregor et al., 2009; Mitchell and Montgomery, 2006; Dunning et al., 2015). The TCN concentration, in this case $^{10}$Be, of the medial moraine sediment reflects the mean concentrations of the source slopes. Due to the stochastic nature of rockwall slope erosion, the spatial distribution of $^{10}$Be concentrations for the source slopes is unlikely to be uniform. The mean concentrations of these slopes are instead considered steady in time and linked to the mean erosion rate (Ward and Anderson 2011). The longer the rockwall slopes are exposed to cosmic rays before the debris is transferred to the glacier surface, the greater the $^{10}$Be concentration in the sediment and therefore the slower the inferred rockwall slope erosion rate. Further details of this methodology and its assumptions are provided by in Supplementary Item 1 and in Ward and Anderson (2011) and Sarr et al. (2019).

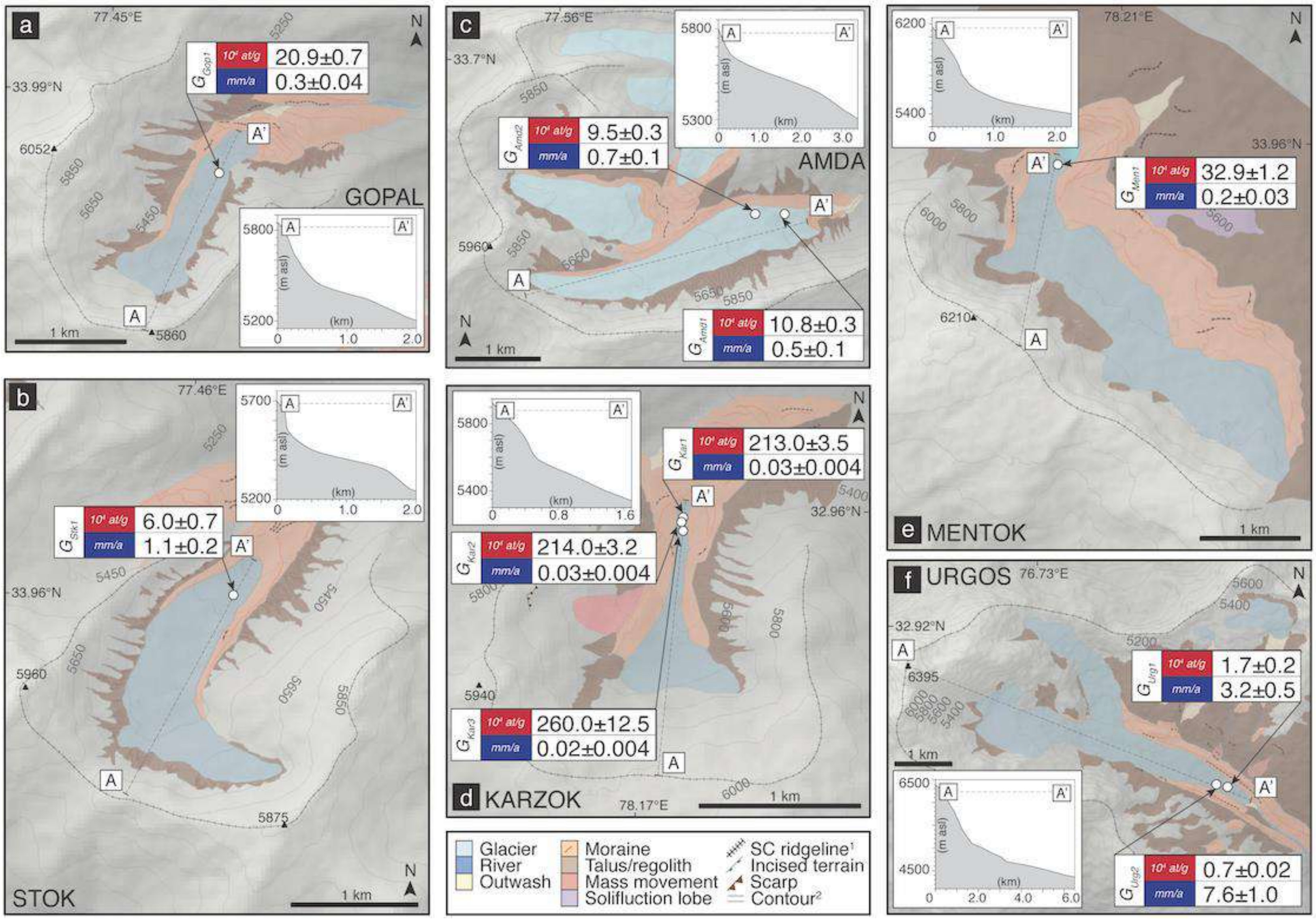
a
GOPAL
77.45°E
33.99°N
6052
5860
$G_{Gop1}$
$10^4$ at/g 20.9±0.7
mm/a 0.3±0.04
1 km
b
STOK
77.46°E
33.96°N
5960
5875
$G_{Stk1}$
$10^4$ at/g 6.0±0.7
mm/a 1.1±0.2
1 km
c
AMDA
77.56°E
33.7°N
5960
$G_{Amd2}$
$10^4$ at/g 9.5±0.3
mm/a 0.7±0.1
$G_{Amd1}$
$10^4$ at/g 10.8±0.3
mm/a 0.5±0.1
1 km
d
KARZOK
78.17°E
32.96°N
5940
$G_{Kar1}$
$10^4$ at/g 213.0±3.5
mm/a 0.03±0.004
$G_{Kar2}$
$10^4$ at/g 214.0±3.2
mm/a 0.03±0.004
$G_{Kar3}$
$10^4$ at/g 260.0±12.5
mm/a 0.02±0.004
1 km
e
MENTOK
78.21°E
33.96°N
6210
$G_{Men1}$
$10^4$ at/g 32.9±1.2
mm/a 0.2±0.03
1 km
f
URGOS
76.73°E
32.92°N
6395
$G_{Urg1}$
$10^4$ at/g 1.7±0.2
mm/a 3.2±0.5
$G_{Urg2}$
$10^4$ at/g 0.7±0.02
mm/a 7.6±1.0
1 km
(m asl)
(km)
Glacier
River
Outwash
Moraine
Talus/regolith
Mass movement
Solifluction lobe
SC ridgeline[1]
Incised terrain
Scarp
Contour[2]

253
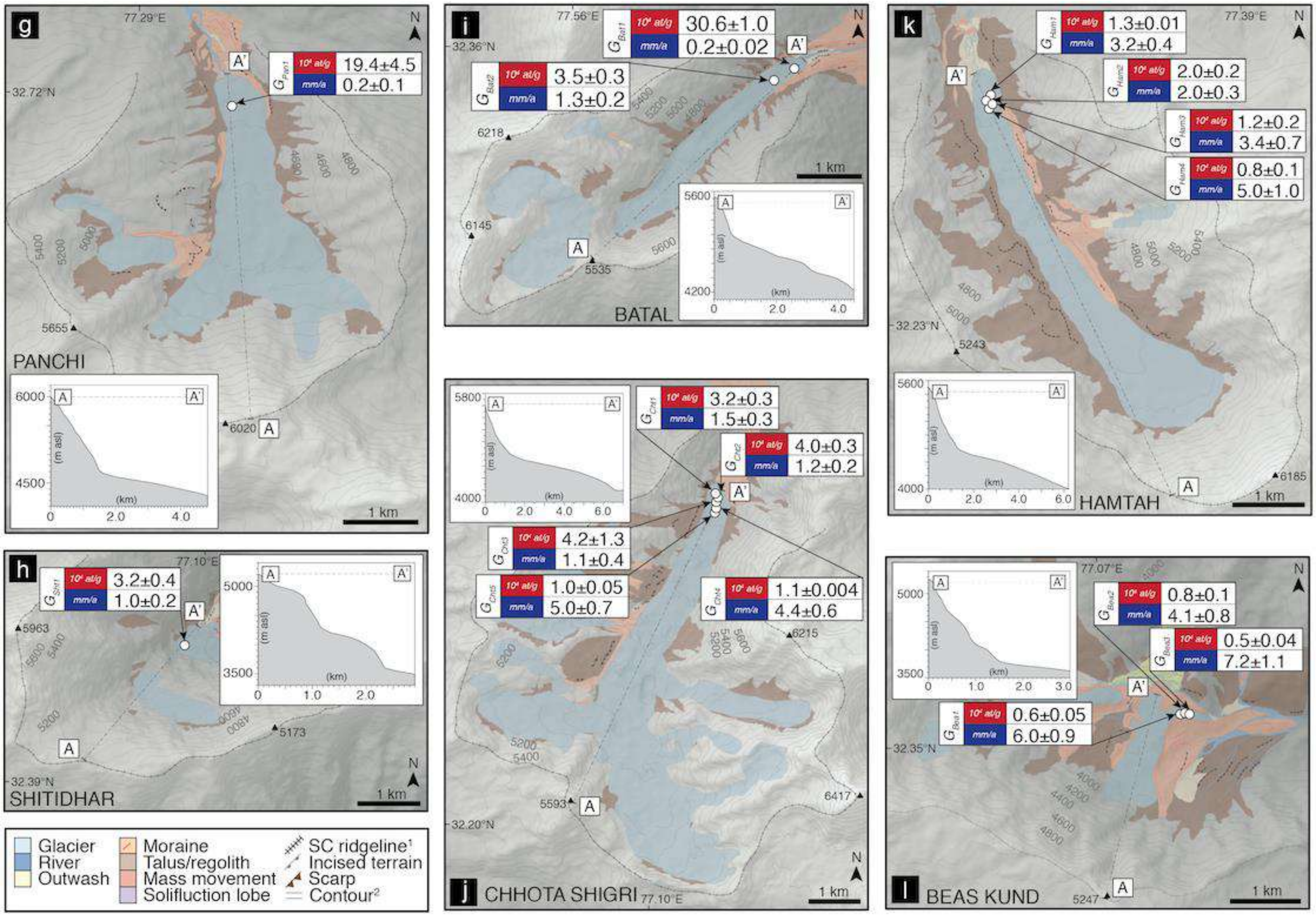
g
PANCHI
19.4±4.5
0.2±0.1
h
SHITIDHAR
3.2±0.4
1.0±0.2
i
BATAL
30.6±1.0
0.2±0.02
3.5±0.3
1.3±0.2
j
CHHOTA SHIGRI
3.2±0.3
1.5±0.3
4.0±0.3
1.2±0.2
4.2±1.3
1.1±0.4
1.0±0.05
5.0±0.7
1.1±0.004
4.4±0.6
k
HAMTAH
1.3±0.01
3.2±0.4
2.0±0.2
2.0±0.3
1.2±0.2
3.4±0.7
0.8±0.1
5.0±1.0
l
BEAS KUND
0.8±0.1
4.1±0.8
0.5±0.04
7.2±1.1
0.6±0.05
6.0±0.9
Glacier
River
Outwash
Moraine
Talus/regolith
Mass movement
Solifluction lobe
SC ridgeline¹
Incised terrain
Scarp
Contour²

**Fig. 2.** Geomorphic maps of the study areas including sample $^{10}$Be concentrations and rockwall slope erosion rates. 1: Catchment ridgeline (encompasses source rockwall slopes). 2: 100-m-contour lines. Alluvial fan deposits in 3l are represented by dark yellow shading.

Orr et al. (2019) argue that the rates of rockwall slope erosion in the upper Bhagirathi catchment in the Uttarkashi district of Uttarakhand are best represented by the erosion rates derived from the centermost medial moraine of Gangotri glacier. This is because the $^{10}$Be concentrations of the moraine fall within uncertainty of each other, and that the other moraines are shown to receive input from the lateral moraines and hillslopes along the ablation zone of the glacier. The study recommends that multiple samples should be taken from each medial moraine and/or glacier to constrain and evaluate any variability in slope erosion throughout the catchment headwaters. Two or less samples are only appropriate when the medial moraine is well preserved with steep relief ridges, has no interaction with ablation zone slopes and where other sampling locations do not fit these criteria. With these recommendations in mind, we carefully collected between one and five samples from stable and well-defined medial moraine ridges for the 12 catchments we investigated (Figs. 2, 3). Each sample location is ≥ 200 m$^2$ in area, to avoid sampling from a single source slope or rockfall event (see Supplementary Item 1). Approximately 3 kg of sediment with a grain size of <3 cm (clay-coarse gravels) was collected for each sample using bulk sediment sampling methods of Gale and Hoare (1991). Detrital samples of this grainsize are shown to effectively infer time-averaged erosion rates, and for this study, are representative of the processes that contribute to rockwall denudation (Lal, 1991; Seong et al., 2009; Delunel et al., 2010). Each sample was named using the initial term ‘G’ for ‘glacier’ followed by an abbreviated term for the catchment name. The samples were numbered in ascending order from the glacier snout, for glaciers with more than one sample. For example, the $G_{Cht1}$ sample was located closest to the snout of Chhota Shigri in Lahul-Spiti, whilst $G_{Cht5}$ was located furthest up-glacier.

To avoid possible bias in the contribution of a particular grain size to the geochemical analyses, we crushed each sample in the Sedimentology Laboratories at the University of Cincinnati. Each amalgamated sample was sieved and the 250–500 μm fraction was retained for $^{10}$Be processing. The extraction of quartz and $^{10}$Be isolation and purification was conducted at the Geochronology Laboratories at the University of Cincinnati, using the chemical procedures of Nishiizumi et al. (1989), von Blanckenburg et al. (2004) and Wittmann et al. (2016). The $^{10}$Be/$^{9}$Be was measured using accelerator mass spectrometry at the Purdue Rare Isotope Measurement (PRIME) Laboratory at Purdue University (Sharma et al., 2000). Native $^{9}$Be was measured via CP–OES for each sample upon the recommendations of Portenga et al. (2015). The total $^{9}$Be, including native $^{9}$Be, rather than just the $^{9}$Be carrier, was then used to calculate the $^{10}$Be concentrations for the dataset.

Ward and Anderson (2011) developed an analytical expression to quantify the accumulation of cosmogenic nuclides during the transport of sediment from the source slopes to the medial moraine. They found that $^{10}$Be accumulation during the burial, englacial transport and exhumation of sediment to the glacier surface was negligible in landscapes with denudation rates ≤ 1 mm/a. This model was implemented in our study because some of the records of erosion local to our investigated catchments, particularly in Uttarakhand, exceed this threshold (0.13–5.37 mm/a; Vance et al., 2003; Lupker et al., 2013; Scherler et al., 2014). Moreover, the glaciers of this study share similar glacier geometries, surface velocities and debris cover characteristics as to those described in the Ward and Anderson (2011) study. The modelled $^{10}$Be accumulation during this transport was then subtracted from the total $^{10}$Be sample concentration for each sample, before deriving the rockwall erosion rates.

Rockwall slope erosion rates were calculated from the $^{10}$Be concentrations and source area production rates using the methods described in detail by Lal (1991), Granger et al. (1996), Balco et al. (2008) and Dortch et al. (2011a). A 1σ uncertainty was propagated through each of the erosion rate calculations. Berylium-10 production rates were calculated for each rockwall slope using a combination of Delunel et al. (2010) and Dortch et al. (2011) codes in MATLAB R2017.a, a calibrated sea-level high-latitude $^{10}$Be spallogenic production rate from Martin et al., (2017; http://calibration.ice-d.org/) and a $^{10}$Be half-life of 1.387 Ma (Korschinek 2010, Chmeleff 2010). Corrections for topographic shielding were made. In Uttarakhand, Scherler et al. (2014) estimated the impact of snow shielding on nuclide concentrations using remote sensing derived observations of snow cover duration and field-based measurements of annual daily snow depth. This data is unavailable for our study area. Widespread avalanching and minimal snow retention on the rockwall slopes for our study areas reduces our concern about the effects of snow shielding. However, we have applied a 5.3% correction to our TCN results; the mean correction value made by Scherler et al. (2014) for ten catchments with similar topographic and climatic characteristics to our study area. This correction does not change any broad trends in the erosion dataset. However, due to the ambiguity attached to these correction estimates, we prefer to refer only to the uncorrected erosion rates herein.

We calculated the Pearson Correlation Coefficient values ($p$) between the $^{10}$Be rockwall slope erosion rates and climatic, topographic and geologic parameters, and conducted Principle Component Analysis (PCA) to identify and evaluate the possible controls of rockwall slope erosion in the NW Himalaya (The R Core Team, 2018; Supplementary Items 3, 4). A $p$-value of $<0.01$ (at $>99\%$ confidence level) was applied. This approach has been successfully applied in other studies to identify and evaluate the nature and magnitude of the environmental and landscape response to changes in climate (Edwards and Richardson 2004; Sagredo and Lowell, 2012; Seaby and Henderson, 2014). The topographic parameters include: catchment and glacier area, mean catchment, rockwall and glacier slope, catchment 3-km-radius relief, mean catchment elevation and snowline altitude and glacier aspect. Climatic variables include: mean annual precipitation (weather stations [as referenced in Table 1] and TRMM [1998−2009]) and temperature (weather stations and

CRU2.0 [as referenced in Table 1]), mean rockwall slope temperature and minimum catchment temperature. Catchment specific temperatures were calculated using an adiabatic lapse rate of 7°C/km and methods outlined in Orr et al. (2019). Additional variables, such as sample grain size and mean apatite fission track (AFT) cooling age (as referenced in Table 5), were also included within these analyses. The latter enables us to identify correlations between modern erosion rates and regional denudation histories on the million-year timescale. The Uttarkashi dataset was not included in these analyses because the rockwall slope erosion rates characterize an extensive basin system with numerous tributary catchments, rather than a single catchment. The basin is examined in more detail in the discussion section below. *P*-values were also calculated between rockwall slope erosion rates and catchment parameters for Ladakh and Lahul-Spiti as discrete regions (Supplementary Item 4). The other studied districts were not subject this regional analysis because the datasets are restricted to only one or two catchments.

## 4. Results

Catchment relief is subdued in the Ladakh region study areas in Jammu and Kashmir (0.7−1.0 km), despite the imposing, high-altitude mountain peaks and rockwalls (>5500 m asl) that mark the headwater limits of each catchment (Table 2). The mean rockwall slopes range between 26.3±12.4 and 35.2±15.5°. The topography of the Lahul-Spiti region in Himachal Pradesh is more severe than Ladakh, even with lower mean elevations (<4500 m asl); the investigated catchments are larger (13.9−44.9$km^2$), and have greater relative relief (1.2±0.3−1.8±0.5 km) and mean rockwall slopes (32.8±12.8−47.2±11.9°).

**Table 2.** Catchment and glacier characteristics of the investigated catchments (uncertainties are expressed to 1σ).

**Table 3**. Medial moraine morphology and sediment descriptions.

**Table 4.** Medial moraine sample details, $^{10}$Be concentrations and inferred rockwall slope erosion rates for the investigated catchments

The ablation zone of the Lahul-Spiti and Kullu glaciers are partially to completely covered by debris, whereas in Ladakh, <30% of the glacier surfaces are covered (Fig. 3; Table 3). Beryllium-10 sample concentrations for the Ladakh and Lahul-Spiti/Kullu catchments range from 6.0±0.7x$10^4$ to 260.0±12.5x$10^4$ at/g and 0.5±0.04x$10^4$ to 30.6±1.0x$10^4$ at/g, respectively (Fig. 2; Table 4). For each catchment, the accumulation of $^{10}$Be during transport between source slopes and the medial moraine was <3 % of the total concentration of each sample (Table 4; Supplementary Item 1). In the Batal catchment, for example, 0.02x$10^4$ at/g of accumulated $^{10}$Be during transport was accounted for when calculating the total sample concentrations of $G_{Bat1}$ (30.6±1.0x$10^4$ at/g) and $G_{Bat2}$ (3.5±0.3x$10^4$ at/g). Beryllium-10 accumulation during this transport for each catchment had a negligible impact on the derived slope erosion rates. Native $^{9}$Be in each sample was either absent or very low (Table 4). The Chhota Shigri $G_{Cht4}$ sample measured the highest amount of native $^{9}$Be in this study at 40.5 ug/g; the correction altered the erosion rate by <1 %.

The $^{10}$Be concentrations in the northern Zanskar Range, Ladakh are 20.9±0.7x$10^4$ at/g for Gopal and 6.0±0.7x$10^4$ at/g for Stok; from these we infer erosion rates of 0.3±0.04 and 1.1±0.2 mm/a, respectively (Figs. 2, 4; Table 4). Erosion rates of 0.7±0.1 and 0.5±0.1 mm/a for the Amda catchment are derived from $^{10}$Be concentrations of 9.5±0.3x$10^4$ and 10.8±0.3x$10^4$ at/g. In central Zanskar, the Karzok samples record $^{10}$Be concentrations from 213.0±3.5x$10^4$ to 260.0±12.5x$10^4$ at/g, which yield slope erosion rates between 0.02±0.004 and 0.03±0.004 mm/a. The adjacent Mentok catchment has a slope erosion rate of 0.2±0.03mm/a from a $^{10}$Be sample concentration of 32.9±1.2x$10^4$ at/g.


**Fig. 3.** Views of medial moraines and sampling locations for three investigated catchments (white and black dashed lines outline medial moraine ridges). a) Beas Kund medial moraine, b) Sampling of $G_{Bea1}$ in Beas Kund, c) Chhota Shigri medial moraine, d) Sampling of $G_{Cht5}$ of Chhota Shigri, e) Urgos medial moraine, f) Sampling of $G_{Urg2}$.

The $^{10}$Be sample concentrations from Urgos in Lahul-Spiti are 0.7±0.02 x10$^4$ and 1.7±0.2x10$^4$ at/g; we infer rockwall slope erosion rates of 7.6±1.0 and 3.2±0.5 mm/a (Table 4). The rate of slope erosion in the Panchi catchment is 0.2±0.1 mm/a, derived from a $^{10}$Be concentration of 19.3±4.5x10$^4$ at/g. For Shitidhar, the $^{10}$Be concentration and derived erosion rate of $G_{Sht1}$ is 3.2±0.4x10$^4$ at/g and 1.1±0.2 mm/a, respectively. The $^{10}$Be sample concentrations range from 3.5±0.3x10$^4$ to 30.6±1.0x10$^4$ at/g and the slope erosion rates range from 0.2±0.02 to 1.4±0.2 mm/a in the Batal catchment. The five samples from the Chhota Shigri catchment have $^{10}$Be concentrations between 1.0±0.05x10$^4$ and 4.2±1.3 x10$^4$ at/g, which yield slope erosion rates between 1.2±0.4 and 5.1±0.7 mm/a. The $^{10}$Be sample concentrations range from 0.8±0.1x10$^4$ to 2.0±0.2x10$^4$ at/g and the slope erosion rates range from 2.1±0.4 to 5.5±1.1 mm/a in Hamtah. For

Beas Kund in the Kullu district, the $^{10}$Be concentrations range from 0.5±0.04x10$^4$ to 0.8±0.1x10$^4$ at/g which derive erosion rates between 4.0±0.7 and 6.8±1.0 mm/a (Table 3).

**Table. 5.** Pearson's Correlation Coefficient values (*p*) between $^{10}$Be rockwall slope erosion rates and catchment parameters.

The strongest statistically significant relationships between rockwall slope erosion and catchment parameters include mean rockwall slope, mean catchment and snowline elevation, mean annual precipitation, mean annual temperature and mean AFT cooling age (Table 5). For the district-specific analysis, the same parameters are strongly correlated with slope erosion in Ladakh ($p$= <0.01; Supplementary Item 4). No parameters statistically correlate with the erosion rates for the Lahul-Spiti district.

## 5. Discussion

In view of the inherent complexities of periglacial-glacial environments and the application of cosmogenic nuclide analysis in these settings, the $^{10}$Be concentrations within each medial moraine dataset are broadly similar (Fig. 4). No relationship is apparent between nuclide concentration and proximity of sample location to either a glacier margin or snout. Any variability in concentrations within the catchments is likely because the medial moraine sediment is poorly mixed and/or has a non-proportional sediment supply that is dominated by stochastic rockfall events (Small et al., 1997; Muzikar, 2008; Ward and Anderson, 2011). The $^{10}$Be concentrations from the Lahul-Spiti and Kullu catchments in Himachal Pradesh are broadly comparable to those from Uttarakhand (<3x10$^4$ at/g), with the exception of Batal and Panchi at the southern margin of the GHS-N unit, where concentrations exceed ~10x10$^4$at/g. Nuclide concentrations from catchments in Ladakh and Shigar either equal or exceed those from northern Lahul-Spiti (Table 4; Figs. 2, 4).

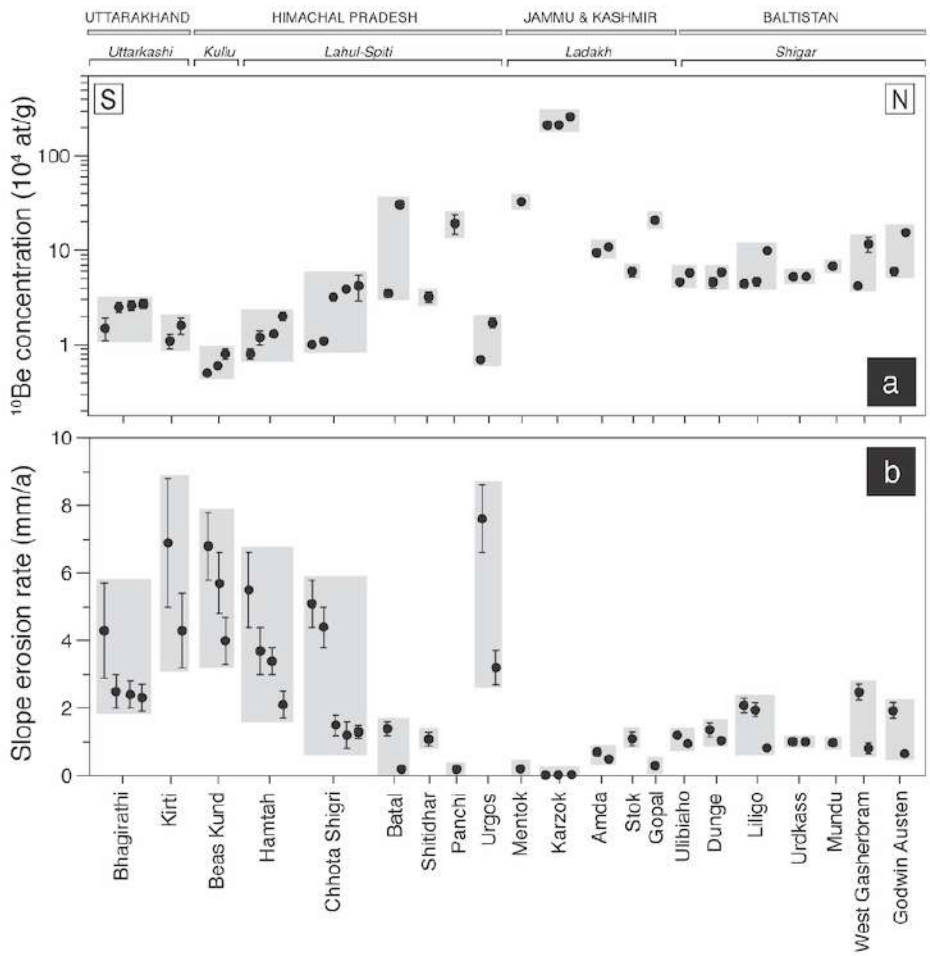


**Fig. 4.** Sample $^{10}$Be concentrations (a) and rockwall slope erosion rates (b) for the NW Himalaya. Uttarkashi and Shigar datasets are from Orr et al. (2019) and Seong et al. (2009), respectively.

The strong variability in physical settings of the catchments prevent any meaningful interpretations or comparisons between specific erosion rates. Moreover, time-averaged nuclide derived erosion rates come with large uncertainties when characterizing local areas ($\leq 10^1$ km$^2$), which has been shown to underestimate the true rates (Yanites et al., 2009; Willenbring et al., 2013; Sadler and Jerolmack, 2014). Instead, we focus on the broad trends of this rockwall slope erosion dataset for the NW Himalaya. Rockwall slope erosion decreases with distance north from the MCT; up to two orders of magnitude difference in erosion exist between Uttarakhand, Himachal Pradesh, Jammu and Kashmir and Baltistan (Fig. 4). The Urgos catchment in northern Lahul-Spiti slightly deviates from this trend with erosion rates of 3.2±0.5 and 7.6±1.0 mm/a, which are equivalent to those records in Kullu and southern Lahul-Spiti. The elevated rates may be attributed to increased annual precipitation in Miyar, which exceeds much of Lahul-Spiti (snowfall: 120−400 cm/a; Patel et al., 2018) and allows for more rapid erosion. Alternatively, the low $^{10}$Be concentrations could be due to the input of fresh debris from the large, steep relief lateral moraines along Urgos glacier (Fig. 3e, f).

The applicable timescales of this time-averaged dataset, although varied (~0.1−24.6 ka), mean that the erosion rates encompass recognized shifts in climate, sediment flux, glacier mass balance and seismicity, which themselves operate across various timescales ($10^{1-6}$ years; Barnard et al., 2001; Finkel et al., 2008; Owen and Dortch, 2014; Scherler et al., 2015). Between ~0.02 and ~8 m of lateral rockwall slope erosion is possible for a single millennium in the NW Himalaya. When these rates are extrapolated for the whole Quaternary, an estimated ~2 km of rockwall retreat is accomplished in the NW Himalaya, which are similar estimates to the Sierra Nevada in the Western USA (Brocklehurst and Whipple, 2002). The magnitude of rockwall slope erosion observed in the NW Himalaya not only demonstrates the importance of slope erosion through periglacial processes, specifically frost cracking in high-altitude alpine settings, but also the significance that localized erosion has for understanding wider landscape change (Small and Anderson 1998; Hales and Roering, 2005, 2007; Moore et al., 2009; Sanders et al., 2012, 2013). The rates of slope erosion reflect, in part, the pace of topographic change at the catchment headwaters.

The magnitude of erosion, particularly in the GHS-S, is sufficient to affect the strength of hillslope-glacier coupling, catchment sediment flux and contribute to topographic change such as the production of relief, the migration of catchment divides, and the reconfiguration of drainage basins (Oskin and Burbank, 2005; Naylor and Gabet, 2007; Heimsath and McGlynn, 2008; MacGregor et al., 2009 *ibid*). The slope erosion rates share a significant association with mean rockwall slope: the greater the mean slope, the more rapid the erosion (Fig. 5a, Table 5). This points to important feedbacks between these variables, where the slope angle and erosion rate limit one another. A tentative relationship can be recognized between relative relief and slope erosion; where catchments with the high-altitude peaks (>5800 m asl), narrow ridgelines and high relief (>1.2±0.2 km), record the highest rates of erosion. Part of this is because catchments with rockwall slope erosion rates >1 mm/a have mean rockwall slopes that exceed the 35° threshold, above which slopes are unable to retain regolith, snow or ice (Gruber and Haerberli, 2007; Nagai et al., 2013). This means that rockfall and avalanching is pervasive. More extensive glacier debris cover in these catchments compared to those with slower erosion demonstrate that coupling between slope and glacier is enhanced in catchments with steep accumulation areas, and that slope is important in moderating hillslope debris flux (Regmi and Watanabe, 2009; Scherler et al., 2011; Table 3). Other studies also recognize the importance of slope in landscape change, some of which argue that slope gradients can be used to infer rates of background denudation (Portenga and Bierman, 2001; Finlayson et al., 2002; Burbank et al., 2003; Ouimet et al., 2009; Scherler et al., 2011, 2014).

Rates of rockwall slope erosion in Uttarkashi and Ladakh districts are either equivalent to, or exceed by up to one order of magnitude, the local catchment-wide erosion and exhumation rates (Fig. 6). Quaternary exhumation rates range between ~0.1 and 3 mm/a in the study areas (Thiede et al., 2004; Theide and Ehlers, 2013). Catchment-wide rates for the Lahul-Spiti and Kullu districts are unavailable because much of the region remains glaciated (Owen and Dortch, 2014). Orr et al. (2019) caution that comparing these erosion datasets can be problematic as they refer to landscape change through a variety of erosional processes and across various spatial and temporal scales. Nevertheless, the order of magnitude difference in these rates show that erosion at catchment headwaters in the NW Himalaya largely outpace the entire drainage basins (Oskin and Burbank, 2005; Naylor and Gabet, 2007), and that erosion can vary significantly across short distances downstream (Scherler et al., 2014). Time-averaged rates for small areas such as catchment headwaters and rockwall slopes are sensitive to short-term local change, including single mass wasting events, and are therefore expected to record more rapid rates of erosion than a catchment-wide perspective (Yanites et al., 2009; Willenbring et al., 2013). The Karzok catchment in central Zanskar of Ladakh deviates from this trend as the rockwall slope erosion either equals or is slower than the catchment-wide erosion and exhumation rates (Fig. 5). The preservation and gradual reworking of landforms and sediment deposits that date to > 400 ka is likely affected by the low background denudation recorded in this region (Hedrick et al., 2011). A possible explanation is that sediment residence times exert a stronger control on the catchment-wide erosion signal in these ancient landscapes than the scale and various surface processes operating in the catchment area.

### *5.2. Controls of slope erosion*

Considerable efforts have been made in recent years to define the parameters that control hillslope stability, and therefore determine the frequency and magnitude of mass wasting events (Matsuoka, 2001; Ballantyne, 2002; Hales and Roering, 2005; Regmi and Watanabe, 2009; Fischer et al., 2006, 2012; Sanders et al., 2012, 2013 *ibid*). The interactions between topography, climate, hydrology, geologic setting and cryosphere dynamics are shown to control rockfall activity. Of the catchment parameters that can be defined in the NW Himalaya, mean rockwall slope as already discussed, mean catchment and snowline elevation, mean annual precipitation, mean annual temperature, and mean AFT cooling ages show the strongest correlation with rockwall slope erosion rates (Figs. 5, 7; Table 5).

Catchments with the most rapid slope erosion have a greater proportion of the rockwall slope above the snowline, and large glacier accumulation areas. Aided by steep slopes that are set in part by erosion, snow and ice entrained with debris is either absent from the rockwall or removed through avalanching. This supports the view that the extent of snow cover, whether set by climatic conditions or surface uplift, is important in moderating mass wasting processes, and can affect the strength of coupling between the rockwall and the glacier system (Scherler et al., 2011, 2014).

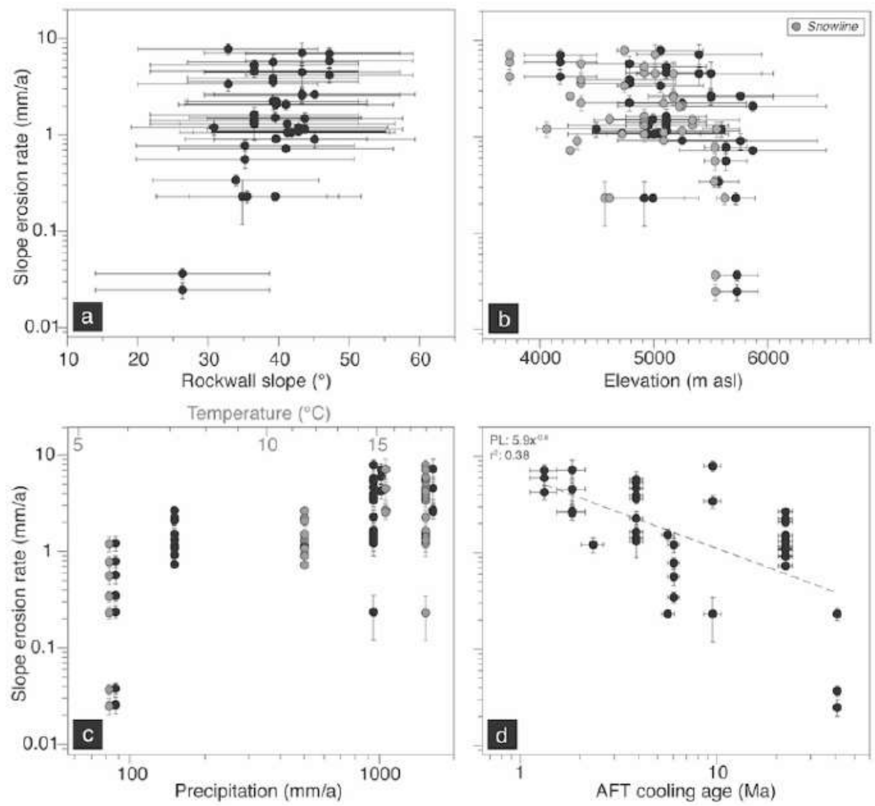


**Fig. 5.** Rockwall slope erosion rates and catchment parameters. a) Mean rockwall slope. b) Mean elevation (black points) and snowline elevation (gray points). c) Mean annual precipitation (black points) and mean annual temperature (gray points). d) Mean AFT cooling ages. (PL: Power Law function).

Estimated surface temperatures of the rockwalls are similar to those considered optimal for mechanical weathering processes (-8 to -3°C), e.g. freeze-thaw, frost cracking and frost wedging (Brozović et al., 1997; Matsuoka and Sakai, 1999; Matsuoka, 2001; Hewitt, 2002; Hales and Roering, 2005; MacGregor et al., 2009; Table 1). The medial moraine sediment characteristics are consistent with sediment from the supraglacial realm, which have detached from source slopes by periglacial weathering processes (Benn and Lehmkuhl, 2000; Schroder et al., 2000; Benn and Owen, 2002; Hambrey et al., 2008; Lukas et al., 2012; Orr et al., 2019; Table 3; Supplementary

Item 5). Rates of periglacial erosion are likely further enhanced by seasonal and/or diurnal thermal variability in exposed bedrock surfaces of our investigated catchments, which is determined in part by the topographic steepness (Gruber and Haerberli, 2007; Fischer et al., 2012; Nagai et al., 2013; Haeberli et al., 2017). However, for high elevation catchments (> 4000 m asl) and/or rockwalls, which lack an insulating layer of snow due to threshold slopes, bedrock surfaces can reach temperatures below -8 °C, which inhibit further mass wasting (Ward and Anderson, 2011). This is tentatively reflected in the relationship between temperature and rockwall slope erosion; the catchments with lower regional temperatures record higher medial moraine $^{10}$Be concentrations and therefore slower erosion rates (Fig. 5c). The rockwall debris flux of each catchment is therefore likely influenced by the feedbacks between elevation, temperature and slope.

A strong negative relationship between $^{10}$Be-derived rockwall slope erosion and mean annual precipitation supports the view that the distribution and magnitude of Himalayan erosion and denudation is partly a function of orographically focused monsoon rainfall (Bookhagen et al., 2005a; Theide et al., 2004; Bookhagen and Burbank, 2006; Gabet et al., 2006; Wulf et al., 2010; Dey et al., 2016; Figs. 5c, 6). The argument that precipitation provides a first-order control on the frequency and magnitude of mass wasting events in alpine settings is common (Hovius et al., 2000; Iverson, 2000; Dortch et al., 2009). Work by Eppes and Keanini (2017) argue that the proficiency of mechanical weathering processes such as sub-critical cracking is climate-dependent, and specifically limited by moisture. Although rockwall slope erosion is certainly influenced by the availability of moisture and is sensitive to the microclimatic conditions of each catchment, its distribution throughout the NW Himalaya cannot be fully explained by precipitation. A five-fold

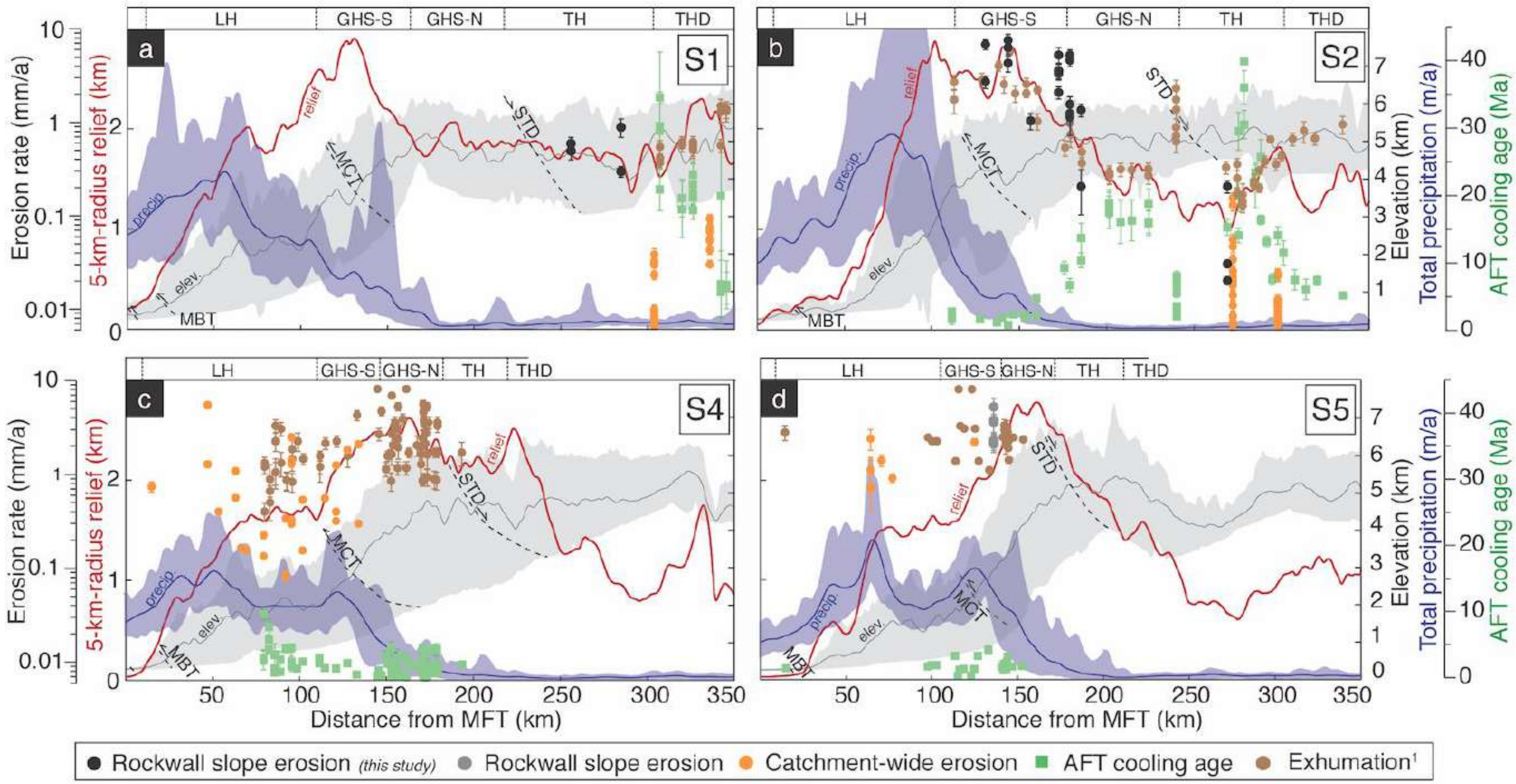


**Fig. 6.** Erosion, relief and precipitation of the NW Himalaya with distance from the MFT (datasets from Bookhagen and Burbank 2010). Swath locations outlined in Fig. 1. Exhumation[1]: Exhumation rates (use erosion rate y-axis) are inferred from AFT cooling ages as referenced below, an AFT cooling temperature of 120°C, and a geothermal gradient of 25°C/km. a) Swath 1 (S1). Rockwall slope erosion: *this study*; catchment-wide erosion: Dortch et al. (2011a), Dietsch et al. (2015); AFT cooling ages: Kristein et al. (2006, 2009). b) Swath 2. Rockwall slope erosion: *this study*, Scherler and Egholm (2017); Kristein et al. (2006, 2009).

b) Swath 2 (S2). Rockwall slope erosion: *this study*, Scherler and Egholm (2017); AFT cooling ages: Schlup et al. (2003, 2011), Thiede et al. (2006), Walia et al. (2008). c) Swath 4 (S4). Catchment-wide erosion: Scherler et al. (2014); AFT cooling ages: Jain et al. (2000), Thiede et al. (2004, 2005, 2009), Vannay et al. (2004). d) Swath 5 (S5). Rockwall slope erosion: Orr et al. (2019); catchment-wide erosion: Vance et al. (2003), Lupker et al. (2012); AFT cooling ages: Sorkhabi et al. (1996), Searle et al. (1999), Thiede et al. (2009).

decline is precipitation occurs between the first topographic high of the Lesser Himalaya (900±400 m asl) and the interior ranges of the orogen (Bookhagen et al., 2005a, b; Bookhagen and Burbank, 2006; Fig. 6). If precipitation were the primary control of rockwall slope erosion we would expect to find that our maximum erosion rates coincide with maximum rainfall, and that a notable decline in these rates would be observed with distance north into the Greater Himalayan interior. However, our results show that this is not the case. Scherler et al (2014) make a similar observation, where the highest catchment-wide rates in Garhwal are also located north of the precipitation maxima. To further emphasize this point, there is an order of magnitude difference in the rockwall slope erosion rates between the GHS-N and the Tethyan Himalayan, yet a small decline in annual precipitation of < 300 mm.

Since the late Miocene the steep orographic barrier of the Himalaya has restricted the northward advancement of moisture (Bookhagen et al., 2005a; Wulf et al., 2010), therefore preventing any subsequent major shift in the overall intensity or distribution of precipitation (Bookhagen et al., 2005a; Bookhagen and Burbank, 2010; Boos and Kuang, 2010; Thiede and Ehlers, 2013). The overall pattern in slope erosion throughout the NW Himalaya is therefore unlikely to be an artefact of a previous climatic regime, despite short-term fluctuations in monsoon strength during the Quaternary potentially affecting rockfall activity on the catchment scale (Thompson et al., 1997; Gupta et al., 2003; Fleitmann et al., 2003; Demske et al., 2009). One major concern in evaluating the role of climate in long-term landscape change is that the denudation records are averaged across million-year timescales and are therefore unable to account for the importance or variations in the

Indian summer monsoon (Bookhagen et al., 2005a; Thiede and Ehlers, 2013). This study is able to show that erosion records that reflect landscape change on timescales that would be sensitive to fluctuations in monsoon strength ($10^{2–5}$ years), i.e. slope and catchment-wide erosion, are not unilaterally controlled by precipitation.

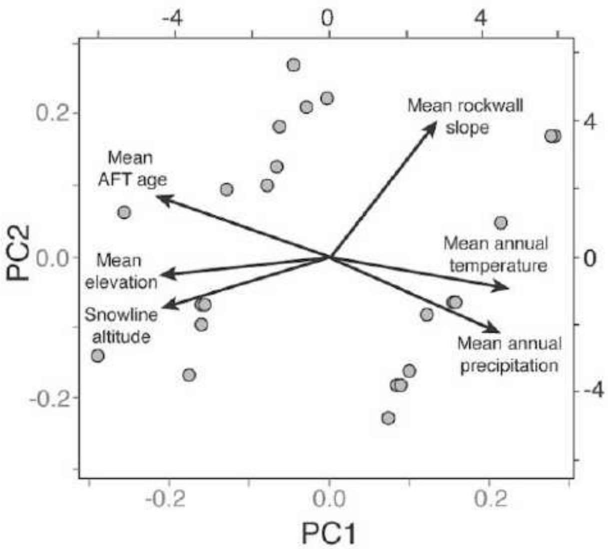


**Fig. 7.** PC1/PC2 plot for the parameters that contribute to the distribution and magnitude of the rockwall slope erosion. Parameters with strongest linear correlation with erosion are labeled. Proportion of variance: PC1 (0.68), PC2 (0.17), PC3 (0.07), PC4 (0.04).

The patterns in rockwall slope erosion rates are most closely associated with regional AFT cooling ages (Figs. 5d, 6; Table 5). Much attention has been paid to understanding the patterns of cooling ages and exhumations rates in the Himalaya, and the feedbacks between tectonics and climate that are responsible for the distribution and intensity of Himalayan denudation across million-year timescales (Schelling and Arita, 1991; Srivastava and Mitra, 1994; Thiede and Ehlers, 2013). Many studies have argued that this denudation is primarily governed by climate; orographic precipitation causes rapid erosion and exhumation along the Himalayan front and Lesser Himalaya (Zeitler et al., 2001; Thiede et al., 2004; Grujic et al., 2006; Biswas et al., 2007; Sharma et al., 2017; Kumar et al., 2018). However, young AFT ages (<10 Ma) and rapid rates of exhumation throughout the

Lesser Himalaya and GHS-S instead reflect a close interaction between tectonics, denudation and monsoon-enhanced erosion, rather than just the latter (e.g. Wobus et al., 2003; Thiede et al., 2004; Vannay et al., 2004). Coupling between climate and tectonics becomes less evident farther into the Greater Himalayan interior; while the GHS-N becomes progressively more arid, the AFT ages remain <17 Ma and exhumation rates < 5mm/a (Thiede and Ehlers, 2013; Schlup et al., 2003; Fig. 6). The pattern in AFT ages and inferred exhumation histories for the NW Himalaya, like our rockwall slope erosion dataset, cannot therefore be fully explained by precipitation. Instead there is the growing argument that the patterns of Himalayan denudation are instead a function of tectonically controlled rock uplift; the result of crustal wedge deformation from the Indo-Eurasian collision and the flat-ramp-flat geometry of the Main Himalayan Thrust (e.g. Burbank et al., 2003; Bollinger et al., 2006; Herman et al., 2010; Robert et al., 2011; Godard et al., 2014). The lateral and vertical transport of rock over the ramp since the late Miocene has resulted in rapid and continuous exhumation, and the generation of steep topographic relief (Cattin and Avouac, 2000; Godard et al., 2004; Lavé and Avouac, 2000, 2001). Young AFT cooling ages and rapid rates of exhumation are therefore focused throughout the Lesser Himalaya and GHS-S (Fig. 6). This is consistent with the pattern in rockwall slope erosion, therefore indicating that tectonically driven rock uplift throughout the NW Himalaya is likely to provide a major control on patterns of denudation since the late Paleogene, and also influence late Quaternary records of erosion (Scherler et al., 2014). Precipitation therefore is a secondary control.

PCA indicate that ~68% of the variance observed in rockwall slope erosion rates in the NW Himalaya can be explained by the six parameters discussed above (mean rockwall slope, mean catchment and snowline elevation, mean annual precipitation, mean annual temperature and mean AFT age; Fig. 7). Other parameters that were either less statistically significant or could not be included in these analyses may also contribute to slope erosion (Table 5). Rockwall lithology, rock strength and mass quality, and jointing and structure for example, affect the thresholds for mass wasting and have been shown to govern hillslope debris flux and rates of erosion (Hallet et al., 1991; Augustinus, 1995; Anderson, 1998; Hales and Roering, 2005; MacGregor et al., 2009; Fischer et al., 2010). Rockfall activity in the investigated catchments is therefore very likely affected by the erodibility of the rockwall and the periglacial processes acting upon it (Heimsath and McGlynn, 2008; Eppes and Keanini, 2017; Moon et al., 2017). The significance of this parameter in patterns of rockwall slope erosion on the regional scale is however less clear. Previous work has argued that the difference in rock strength between the crystalline sequences of the Lesser and Greater Himalaya is negligible, and has little influence upon the denudation histories of the orogen (Burbank et al., 2003; Scherler et al., 2011, 2014).

Studies throughout High Asia have shown that geomorphic change, specifically mass wasting events, are closely associated with neotectonism including stochastic earthquakes and/or persistent microseismicity (Hovius et al., 2000; Menunier et al., 2008; Dortch et al., 2009; Lupker et al., 2012). For example, earthquakes in Uttarakhand such as the 1991 Uttarkashi (M 6.1; Valdiya, 1991; Bali et al., 2003) and 1999 Chamoli (M 6.6; Rajendran et al., 2000) events are found to trigger mass redistribution on a scale that affects short term erosion rates (Bali et al., 2003; Scherler et al., 2014). The frequency of rockfall events and therefore rates of rockwall slope erosion in our catchments is therefore likely to be influenced in part by local tectonic activity.

A further candidate for rockwall slope erosion control is glaciation and glacial erosion; vertical incision and the debuttressing of slopes can lead to enhanced slope instability and failure (Naylor and Gabet, 2007; Heimsath and McGlynn, 2008; MacGregor et al., 2009; Fischer et al., 2010). Large, erosive temperate glaciers occupy catchments with rapid rates of rockwall slope erosion, while slower rates are from catchments with less erosive, sub-polar glaciers (Owen and Dortch, 2014). Past retreat and expansion of glacier ice may also have contributed to the evolution of the rockwalls; the downwasting of ice may encourage the unloading of slope debris, while a greater glacier volume may see an increase in glacial erosion processes acting upon the slope (Fischer et al., 2006; 2010, 2012; Herman et al., 2017). The erosion record of Karzok for example is representative of rockwall erosion since ~24 ka, which encompasses at least two local glacial stages (Table 1). Saha et al. (2018) argue that these stages amongst others in this region are driven by North Atlantic cooling, teleconnected via the mid-latitude westerlies. Similarly, shifts in glacier mass balance are observed throughout the Late Holocene in catchments with applicable erosion timescales of <1 ka (Table 1). Rockwall slope erosion is therefore likely to contribute to a catchment's response to fluctuations in glacial mass balance over time, which is forced by shifts in climate.

Rather than a single control, we have demonstrated that rockwall slope erosion is instead more likely the result of longstanding feedbacks between climate, tectonics, topography and surface processes. This supports the initial findings of Orr et al. (2019), where the evolution of the rockwalls in the present day is determined by the unique expression of these feedbacks within each catchment. However, our erosion dataset does not account for any variability in the drivers or rate of rockfall activity throughout the applicable timescales (0.1−24 ka). The relative importance of each of these various parameters in rockwall slope erosion will therefore likely vary across spatial and temporal scales. The relationship between rockwall erosion and slope for example, which is recognized for the whole dataset, is not apparent in Lahul-Spiti district, if it is considered discrete region. Only in Ladakh does the steepest catchment and rockwall slopes record the most rapid rates of erosion. No catchment parameters have strong correlations with rockwall slope erosion for Lahul-Spiti. This may be because slope erosion is sensitive to other undefined parameters such as glaciation, or that deciphering erosion controls is not possible due to the inherent complexities of glaciated catchments in the NW Himalaya. An alternative explanation is that once a threshold for a parameter is met, rockwall slope erosion is then predominantly limited by this one parameter. During a period of enhanced rainfall or monsoon along the Himalayan front for example

(Bookhagen et al., 2005b; Clift et al., 2008), catchments with strongly contrasting physical settings may display similar rockfall activity. In this case, the rainfall magnitude is sufficient to override any resistance to mass wasting, such as a strong, non-erosive rock type or shallow, low relief slopes. When averaged over time, these catchments will share a similar record of erosion. This may offer an explanation for why single high-magnitude events such as these, are viewed to be responsible for a significant proportion of the total landscape change in mountain environments (Hasnain 1996; Kirchner et al., 2001; Craddock et al., 2007; Wulf et al., 2010).

We suggest that rockwall slope erosion is largely influenced by catchment-specific conditions that vary over temporal and spatial scales. However, our study is able to demonstrate that the broad spatial patterns in rockwall erosion follow long-term trends in denudation throughout the NW Himalaya, and is therefore broadly controlled by tectonically driven rock uplift. Precipitation is considered a secondary control. This suggests that periglacial rockfall processes are part of the erosional response to structural change throughout the Himalayan-Tibetan orogen, and play a significant role within topographic change at catchment headwaters and the mass balance of the orogen. Identifying a more significant tectonic control to landscape change than climate is becoming more common; work in the wider Himalaya and the northern Bolivian Andes suggest that denudation patterns do not follow gradients in precipitation (Burbank et al., 2003; Gasparini and Whipple, 2014; Godard et al., 2014; Scherler et al., 2014).

## 6. Conclusion

Rates of rockwall slope erosion are defined for 12 catchments in northern India, NW Himalaya and range between 0.02±0.04 and 7.6±1.0 mm/a. Rockwall slope erosion largely outpaces local catchment-wide erosion and exhumation, and is sufficient to affect catchment sediment flux, glacier dynamics and topographic change, such as the production of relief, the migration of catchment divides and the reconfiguration of drainage basins.

Erosion rates become progressively slower with distance north from the MCT; up to two orders of magnitude difference in erosion rates are observed between Uttarkashi, Kullu, Lahul-Spiti, and Ladakh and Shigar. Rather than a single control, rockwall slope erosion on a catchment-by-catchment basis is largely influenced by longstanding feedbacks between climate, tectonics, topography and surface processes. The relative roles of these parameters are likely to vary over various spatial and temporal scales.

Our study demonstrates that like records of denudation in the NW Himalaya, the broad trend in rockwall slope erosion cannot be fully explained by the distribution of precipitation. Instead rockwall slope erosion can be considered part of the erosional response to tectonically driven uplift, the product of Indo-Eurasian convergence and the geometry of overthrusting. The distribution and magnitude of erosion applicable to geomorphic ($10^{2-5}$ years) and geologic ($10^{6}$ years) timescales in the NW Himalaya therefore suggests that tectonics, rather than climate, provide a first-order control on landscape evolution. Our study also demonstrates the importance of lateral rockwall slope erosion via periglacial processes in helping set the pace of topographic change at catchment headwaters of high altitude and high relief mountain ranges, and the significance that localized erosion has for understanding wider landscape change.

## Acknowledgments

Data supporting the conclusions is in the process of being archived with the GFZ Data Services repository (http://dataservices.gfz-potsdam.de/portal/). In the interim and for review purposes, this data can be accessed in Supplementary Items 1–5. The authors acknowledge that this manuscript will not be published until the data is completely archived and publicly available.

ENO thanks the University of Cincinnati for providing tuition and stipend to support this work as part of ENO's doctoral thesis and the processing of samples for $^{10}$Be dating. ENO would like to thank PRIME Laboratories at Purdue University for a seed grant for AMS measurements. ENO also extends thanks to National Geographic, the Geological Society of America and the Graduate Student Governance Association, University of Cincinnati for research grants to conduct fieldwork. ENO and SS thank T. Dorje and Discover Ladakh for providing logistical support in the field.

## References

Adams, B., Dietsch, C., Owen, L.A., Caffee, M.W., Spotila, J., Haneberg, W.C. (2009). Exhumation and incision history of the Lahul Himalaya, northern India, based on (U–Th)/He thermochronometry and terrestrial cosmogenic nuclide methods. *Geomorphology*, 107(3-4),285-299. https://doi.org/10.1016/j.geomorph.2008.12.017

Anderson, R.S. (1998). Near-surface thermal profiles in alpine bedrock: Implications for the frost weathering of rock. *Arctic and Alpine Research*, 30(4), 362-372. https://doi.org/10.1080/00040851.1998.12002911

Anderson, L.S., Roe, G.H., Anderson, R.S. (2014). The effects of interannual climate variability on the moraine record. *Geology*, 42(1), 55-58. https://doi.org/10.1130/G34791.1

Augustinus, C. 1995. Glacial valley cross-profile development: the influence of in situ rock stress and rock mass strength, with examples from the Southern Alps, New Zealand. *Geomorphology*, 14(2), 87-97. https://doi.org/10.1016/0169-555X(95)00050-X

Azam, M.F., Wagnon, , Vincent, C., Ramanathan, A.L., Favier, V., Mandal, A., Pottakkal, J.G. (2014). Processes governing the mass balance of Chhota Shigri Shigri Glacier (western Himalaya, India) assessed by point-scale surface energy balance measurements. *The Cryosphere*, 8(6), 2195-2217. https://doi.org/10.5194/tc-8-2195-2014

Balco, G., Stone, J., Lifton, N., Dunai, T. (2008). A complete and easily accessible means of calculating surface exposure ages or erosion rates from $^{10}$Be and $^{26}$Al measurements. *Quaternary Geochronology*, 3, 174-195. https://doi.org/10.1016/j.quageo.2007.12.001

Bali, R., Awasthi, D.D., Tiwari, N.K. (2003). Neotectonic control on the geomorphic evolution of the Gangotri Glacier Valley, Garhwal Himalaya. *Gondwana Research* 6(4). 829-838. https://doi.org/10.1016/S1342-937X(05)71028-5

Ballantyne, C.K. (2002). Paraglacial geomorphology. *Quaternary Science Reviews*, 21(18-19), 1935-2017. https://doi.org/10.1016/S0277-3791(02)00005-7

Barnard, , Owen, L., Finkel, R. (2004). Style and timing of glacial and paraglacial sedimentation in a monsoon-influenced high Himalayan environment, the upper Bhagirathi Valley, Garhwal Himalaya. *Sedimentary Geology*, 165, 199-221. https://doi.org/10.1016/j.sedgeo.2003.11.009

Barr, I.D., Lovell, H. (2014). A review of topographic controls on moraine distribution. *Geomorphology*, 226, 44-64.https://doi.org/10.1016/j.geomorph.2014.07.030

Bashir, F.,Rasul, G. (2010). Estimation of water discharge from Gilgit Basin using remote sensing, GIS and runoff modeling. *Pakistan Journal of Meteorology*, 6(12).

Benn D.I, Lehmkuhl F. (2000). Mass balance and equilibrium-line altitudes of glaciers in high-mountain environments. *Quaternary International* 65. 15-29. https://doi.org/10.1016/S1040-6182(99)00034-8

Benn, D., Owen, L. (1998). The role of the Indian summer monsoon and the mid-latitude westerlies in Himalayan glaciation: a review and speculative discussion. *Journal of the Geological Society*, 155, 353–363. https://doi.org/10.1144/gsjgs.155.2.0353

Benn, D.I., Owen, L.A. (2002). Himalayan glacial sedimentary environments: a framework for reconstructing and dating former glacial extents in high mountain regions. *Quaternary International*, 97-98, 3-26. https://doi.org/10.1016/S1040-6182(02)00048-4

Benn D.I, Owen L.A, Osmaston H.A, Seltzer G.O, Porter S.C, Mark B. (2005). Reconstruction of equilibrium-line altitudes for tropical and sub-tropical glaciers. *Quaternary International* 138: 8-21. https://doi.org/10.1016/j.quaint.2005.02.003

Benn, D.I., Bolch, T., Hands, K., Gulley, J., Luckman, A., Nicholson, L.I., Quincey, D., Thompson, S., Toumi, R.,Wiseman, S. (2012). Response of debris-covered glaciers in the Mount Everest region to recent warming, and implications for outburst flood hazards. Earth-Science Reviews, 114(1-2), 156-174. https://doi.org/10.1016/j.earscirev.2012.03.008

Biswas S, Coutand I, Grujic D, Hager C, Stöckli D, Grasemann B. (2007). Exhumation and uplift of the Shillong plateau and its influence on the eastern Himalayas: New constraints from apatite and zircon (U-Th-[Sm])/He and apatite fission track analyses. *Tectonics* 26(6). https://doi.org/10.1029/2007TC002125

Bojar, A.V., Fritz, H., Nicolescu, S., Bregar, M., Gupta, R. (2005). Timing and mechanisms of Central Himalayan exhumation: discriminating between tectonic and erosion processes. *Terra Nova*, 17, 5, 427-433. https://doi.org/10.1111/j.1365-3121.2005.00629.x

Bollinger, L., Henry, , Avouac, J. (2006). Mountain building in the Nepal Himalaya: Thermal and kinematic model. *Earth and Planetary Science Letters*, 244(1-2), 58-71. https://doi.org/10.1016/j.epsl.2006.01.045

Bookhagen, B., Burbank, D. (2006). Topography, relief and TRMM-derived rainfall variations along the Himalaya. *Geophysical Research Letters*, 33, 105. https://doi.org/10.1029/2006GL026037

Bookhagen, B., Burbank, D. (2010). Toward a complete Himalayan hydrological budget: Spatiotemporal distribution of snowmelt and rainfall and their impact on river discharge. *Journal of Geophysical Research* 115, F3, 1-25. https://doi.org/10.1029/2009JF001426

Bookhagen, B., Thiede, R., Strecker, M. (2005a). Late Quaternary intensified monsoon phases control landscape evolution in the northwest Himalaya. *Geology* 33, 1, 149-152. https://doi.org/10.1130/G20982.1

Bookhagen, B., Thiede, R.C., Strecker, M.R. (2005b). Abnormal monsoon years and their control on erosion and sediment flux in the high, arid northwest Himalaya. *Earth and Planetary Science Letters*, 231(1-2), 131-146. https://doi.org/10.1016/j.epsl.2004.11.014

Boos, W.R., Kuang, Z. (2010). Dominant control of the South Asian monsoon by orographic insulation versus plateau heating. *Nature*, 463(7278), 218. https://doi.org/10.1038/nature08707

Boulton G.S. (1978). Boulder shapes and grain-size distributions of debris as indicators of transport paths through a glacier and till genesis. *Sedimentology* 25(6). 773-799. https://doi.org/10.1111/j.1365-3091.1978.tb00329.x

Brocklehurst, S.H., Whipple, K.X. (2002). Glacial erosion and relief production in the Eastern Sierra Nevada, California. *Geomorphology*, 42(1-2), 1-24. https://doi.org/10.1016/S0169-555X(01)00069-1

Brocklehurst, S.H., Whipple, K.X. (2006). Assessing the relative efficiency of fluvial and glacial erosion through simulation of fluvial landscapes. *Geomorphology*, 75(3-4), 283-299. https://doi.org/10.1016/j.geomorph.2005.07.028

Brozovic, N., Burbank, D.W., Meigs, A.J., (1997). Climatic limits on landscape development in the northwestern Himalaya. *Science* 276, 571-574. https://doi.org/10.1126/science.276.5312.571

Burbank, D., Blythe, A., Putkonen, J., Pratt-Sitaula, B., Gabet, E., Oskin, M., Barros, A., Ojha, T. (2003). Decoupling of erosion and precipitation in the Himalayas. *Nature* 426, 652-655. https://doi.org/10.1038/nature02187

Cattin, R., Avouac, J. (2000). Modeling mountain building and the seismic cycle in the Himalaya of Nepal. *Journal of Geophysical Research: Solid Earth*, 105(B6), 13389-13407. https://doi.org/10.1029/2000JB900032

Clift, , Giosan, L., Blusztajn, J., Campbell, I., Allen, C., Pringle, M., Tebrez, A., Danish, M., Rabbani, M., Alizai, A., Carter, A., Luckge, A. (2008). Holocene erosion of the Lesser Himalaya triggered by intensified summer monsoon. *Geology* 36, 79-82. https://doi.org/10.1130/G24315A.1

Craddock, W.H., Burbank, D.W., Bookhagen, B., Gabet, E.J. (2007). Bedrock channel geometry along an orographic rainfall gradient in the upper Marsyandi River valley in central

Nepal. *Journal of Geophysical Research: Earth Surface*, 112(F3). https://doi.org/10.1029/2006JF000589

DeCelles, G., Robinson, D.M., Quade, J., Ojha, T., Garzione, C.N., Copeland, , Upreti, B.N. (2001). Stratigraphy, structure, and tectonic evolution of the Himalayan fold-thrust belt in western Nepal. *Tectonics*, 20(4), 487-509. https://doi.org/10.1029/2000TC001226

Deeken, A., Thiede, R.C., Sobel, E.R., Hourigan, J.K., Strecker, M.R. (2011). Exhumational variability within the Himalaya of northwest India. *Earth and Planetary Science Letters*, 305(1-2), 103-114. https://doi.org/10.1016/j.epsl.2011.02.045

Delunel, R., Van Der Beek, P.A., Carcaillet, J., Bourlès, D.L., Valla, P.G. (2010). Frost-cracking control on catchment denudation rates: Insights from in situ produced 10Be concentrations in stream sediments (Ecrins–Pelvoux massif, French Western Alps). *Earth and Planetary Science Letters*, 293(1-2), 72-83. https://doi.org/10.1016/j.epsl.2010.02.020

Demske, D., Tarasov, E., Wünnemann, B., Riedel, F. (2009). Late glacial and Holocene vegetation, Indian monsoon and westerly circulation in the Trans-Himalaya recorded in the lacustrine pollen sequence from Tso Kar, Ladakh, NW India. *Palaeogeography, Palaeoclimatology, Palaeoecology*, 279(3), 172-185. https://doi.org/10.1016/j.palaeo.2009.05.008

Derbyshire, E., Shi, Y., Li, J., Zheng, B., Li, S., Wang, J. (1991). Quaternary glaciation of Tibet: the geological evidence. *Quaternary Science Reviews*. 10, 485-510. https://doi.org/10.1016/0277-3791(91)90042-S

de Scally, F.A. (1997). Deriving lapse rates of slope air temperature for meltwater runoff modeling in subtropical mountains: An example from the Punjab Himalaya, Pakistan. *Mountain Research and Development*, 353-362. https://doi.org/10.2307/3674024

Dey, S., Thiede, R.C., Schildgen, T.F., Wittmann, H., Bookhagen, B., Scherler, D., Jain, V., Strecker, M.R. (2016). Climate-driven sediment aggradation and incision since the late Pleistocene in the NW Himalaya, India. *Earth and Planetary Science Letters*, 449, 321-331. https://doi.org/10.1016/j.epsl.2016.05.050

Dietsch, C., Dortch, J., Reynhout, S., Owen, L., Caffee, M. (2015). Very slow erosion rates and landscape preservation across the southwestern slope of the Ladakh Range, India. *Earth Surface Processes and Landforms*, 40, 3, 389-402. https://doi.org/10.1002/esp.3640

Dortch, J.M., Owen, L.A., Haneberg, W.C., Caffee, M.W., Dietsch, C., Kamp, U. (2009). Nature and timing of large landslides in the Himalaya and Transhimalaya of northern India. *Quaternary Science Reviews* 28, 1037-1056. https://doi.org/10.1016/j.quascirev.2008.05.002

Dortch, J.M., Dietsch, C., Owen, L.A., Caffee, M.W. and Ruppert, K. (2011b). Episodic fluvial incision of rivers and rock uplift in the Himalaya and Transhimalaya. *Journal of the Geological Society*, 168(3), 783-804. https://doi.org/10.1144/0016-76492009-158

Dortch, J., Owen, L., Schoenbohm, L., Caffee, M. (2011a). Asymmetrical erosion and morphological development of the central Ladakh Range, northern India. *Geomorphology* 135, 167-180. https://doi.org/10.1016/j.geomorph.2011.08.014

Dortch, J., Owen, L., Caffee, M. (2013). Timing and climatic drivers for glaciation across semi-arid western Himalayan-Tibetan orogen. *Quaternary Science Reviews* 78, 188-208. https://doi.org/10.1016/j.quascirev.2013.07.025

Edwards, M., Richardson, A.J. (2004). Impact of climate change on marine pelagic phenology and trophic mismatch. *Nature*, 430(7002), 881. https://doi.org/10.1038/nature02808

Eppes, M.C., Keanini, R. (2017). Mechanical Weathering and Rock Erosion by Climate-Dependent Subcritical Cracking. *Reviews of Geophysics*. 55, 470–508. https://doi.org/10.1002/2017RG000557

Finkel, R., Owen, L., Barnard, P., Caffee, M. (2003). Beryllium-10 dating of Mount Everest moraines indicates a strong monsoon influence and glacial synchroneity throughout the Himalaya. *Geology* 31, 6, 561-564. https://doi.org/10.1130/0091-7613(2003)031<0561:BDOMEM>2.0.CO;2

Finlayson D.P, Montgomery D.R, Hallet B. (2002). Spatial coincidence of rapid inferred erosion with young metamorphic massifs in the Himalayas. *Geology* 30(3), 219-222. https://doi.org/10.1130/0091-7613(2002)030<0219:SCORIE>2.0.CO;2

Fischer, L., Kääb, A., Huggel, C., Noetzli, J. (2006). Geology, glacier retreat and permafrost degradation as controlling factors of slope instabilities in a high-mountain rock wall: the Monte Rosa east face. *Natural Hazards and Earth System Sciences,* 6(5), 761-772. https://doi.org/10.5194/nhess-6-761-2006.

Fischer, L., Amann, F., Moore, J.R., Huggel, C. (2010). Assessment of periglacial slope stability for the 1988 Tschierva rock avalanche (Piz Morteratsch, Switzerland). *Engineering Geology*, 116(1-2), 32-43. https://doi.org/10.1016/j.enggeo.2010.07.005

Fischer, L., Purves, R.S., Huggel, C., Noetzli, J., Haeberli, W. (2012). On the influence of topographic, geological and cryospheric factors on rock avalanches and rockfalls in high-mountain areas. *Natural Hazards and Earth System Sciences*, 12(1), 241. https://doi.org/10.5194/nhess-12-241-2012

Fischer, L., Huggel, C., Kääb, A., Haeberli, W. (2013). Slope failures and erosion rates on a glacierized high-mountain face under climatic changes. *Earth surface processes and landforms*, 38(8), pp.836-846, https://doi.org/10.1002/esp.3355

Fleitmann, D., Burns, S.J., Mudelsee, M., Neff, U., Kramers, J., Mangini, A., Matter, A. (2003). Holocene forcing of the Indian monsoon recorded in a stalagmite from southern Oman. *Science* 300, 1737–1739. https://doi.org/10.1126/science.1083130

Foster, D., Brocklehurst, S.H., Gawthorpe, R.L. (2008). Small valley glaciers and the effectiveness of the glacial buzzsaw in the northern Basin and Range, USA. *Geomorphology*, 102(3-4), 624-639. https://doi.org/10.1016/j.geomorph.2008.06.009

Frank, W., Hoinkes, G., Miller, C., Purtscheller, F., Richter, W., Thöni, M. (1973). Relations between metamorphism and orogeny in a typical section of the Indian

Himalayas. *Tschermaks mineralogische und petrographische Mitteilungen*, 20(4), 303-332. https://doi.org/10.1007/BF01081339

Gabet, E.J., Burbank, D.W., Putkonen, J.K., Pratt-Sitaula, B.A., Ojha, T. (2004). Rainfall thresholds for landsliding in the Himalayas of Nepal. *Geomorphology*, 63(3-4), 131-143. https://doi.org/10.1016/j.geomorph.2004.03.011

Gadgil, S. (2003). The Indian monsoon and its variability. *Annual Review of Earth and Planetary Sciences*, 31(1), 429-467. https://doi.org/10.1146/annurev.earth.31.100901.141251

Gale S.J, Hoare G. (1991). Quaternary Sediments: Petrographic Methods for the Study of Unlithified Rocks. Wiley, Chichester.

Gasparini, N.M., Whipple, K.X. (2014). Diagnosing climatic and tectonic controls on topography: Eastern flank of the northern Bolivian Andes. *Lithosphere*, 6(4), 230-250. https://doi.org/10.1130/L322.1

Gibson M.J, Glasser N.F, Quincey D.J, Mayer C, Rowan A.V, Irvine-Fynn, T.D. (2017). Temporal variations in supraglacial debris distribution on Baltoro Glacier, Karakoram between 2001 and 2012. *Geomorphology* 295: 572-585. https://doi.org/10.1016/j.geomorph.2017.08.012

Godard, V., Cattin, R., Lavé, J. (2004). Numerical modeling of mountain building: Interplay between erosion law and crustal rheology. *Geophysical Research Letters*, 31(23). https://doi.org/10.1029/2004GL021006

Godard, V., Bourlès, D.L., Spinabella, F., Burbank, D.W., Bookhagen, B., Fisher, G.B., Moulin, A., Léanni, L. (2014). Dominance of tectonics over climate in Himalayan denudation. *Geology*, 42(3), 243-246. https://doi.org/10.1130/G35342.1

Gupta, A.K., Anderson, D.M., Overpeck, J.T. (2003). Abrupt changes in the Asian southwest monsoon during the Holocene and their links to North Atlantic Ocean. *Nature* 421, 354–357. https://doi.org/10.1038/nature01340

Gruber, S., Haeberli, W. (2007). Permafrost in steep bedrock slopes and its temperature-related destabilization following climate change. *Journal of Geophysical Research: Earth Surface*, 112(F2). https://doi.org/10.1029/2006JF000547

Grujic D, Coutand I, Bookhagen B, Bonnet S, Blythe A, Duncan C. (2006). Climatic forcing of erosion, landscape, and tectonics in the Bhutan Himalayas. *Geology* 34(10): 801-804. https://doi.org/10.1130/G22648.1

Granger, D.E., Kirchner, J.W., Finkel, R. (1996). Spatially averaged long-term erosion rates measured from in situ-produced cosmogenic nuclides in alluvial sediment. *The Journal of Geology*, 104(3), 249-257. https://doi.org/10.1086/629823

Haeberli, W., Schaub, Y., Huggel, C. (2017). Increasing risks related to landslides from degrading permafrost into new lakes in de-glaciating mountain ranges. *Geomorphology*, 293, 405-417. https://doi.org/10.1016/j.geomorph.2016.02.009

Hales, T.C., Roering, J.J. (2005). Climate-controlled variations in scree production, Southern Alps, New Zealand. *Geology*, 33(9), 701-704. https://doi.org/10.1130/G21528.1

Hales, T.C., Roering, J.J. (2007). Climatic controls on frost cracking and implications for the evolution of bedrock landscapes. *Journal of Geophysical Research: Earth Surface*, 112(F2). https://doi.org/10.1029/2006JF000616

Hallet, B, Walder, J.S., Stubbs, C.W. (1991). Weathering by segregation ice growth in microcracks at sustained subzero temperatures: Verification from an experimental study using acoustic emissions. *Permafrost and Periglacial Processes* 2(4): 283-300. https://doi.org/10.1002/ppp.3430020404

Hambrey M.J, Quincey D.J, Glasser N.F, Reynolds J.M, Richardson S.J. Clemmens, S. (2008). Sedimentological, geomorphological and dynamic context of debris-mantled glaciers, Mount Everest (Sagarmatha) region, Nepal. *Quaternary Science Reviews* 27(25-26): 2361-2389. https://doi.org/10.1016/j.quascirev.2008.08.010

Hasnain, S.I. (1996). Factors controlling suspended sediment transport in Himalayan glacier meltwaters. *Journal of Hydrology*, 181(1-4), 49-62. https://doi.org/10.1016/0022-1694(95)02917-6

Hedrick, K., Seong, Y., Owen, L., Caffee, M., Dietsch, C. (2011). Towards defining the transition in style and timing of Quaternary glaciation between the monsoon-influenced Greater Himalaya and the semi-arid Transhimalaya of Northern India. *Quaternary International*, 236, 21-33. https://doi.org/10.1016/j.quaint.2010.07.023

Heimsath, A.M., McGlynn, R. (2008). Quantifying periglacial erosion in the Nepal high Himalaya. *Geomorphology*, 97(1-2), 5-23. https://doi.org/10.1016/j.geomorph.2007.02.046

Herman, F., Copeland, , Avouac, J., Bollinger, L., Mahéo, G., Le Fort, , Rai, S., Foster, D., Pêcher, A., Stüwe, K., Henry. (2010). Exhumation, crustal deformation, and thermal structure of the Nepal Himalaya derived from the inversion of thermochronological and thermobarometric data and modeling of the topography. *Journal of Geophysical Research: Solid Earth*, 115(B6). https://doi.org/10.1029/2008JB006126

Hewitt, K. (2002). Altitudinal organization of Karakoram geomorphic processes and depositional environments. In Himalaya to the sea (118-133). Routledge.

Hodges, K.V. (2000). Tectonics of the Himalaya and southern Tibet from two perspectives. *Geological Society of America Bulletin* 112, 3, 324-350. https://doi.org/10.1130/0016-7606(2000)112<324:TOTHAS>2.0.CO;2

Hodges, K.V., Wobus, C., Ruhl, K., Schildgen, T., Whipple, K. (2004). Quaternary deformation, river steepening, and heavy precipitation at the front of the Higher Himalayan ranges. *Earth and Planetary Science Letters*, 220, 3-4, 379-389. https://doi.org/10.1016/S0012-821X(04)00063-9

Hovius, N., Stark, C., Hao-Tsu, C., Jiun-Chuan, L. (2000). Supply and removal of sediment in a landslide-dominated mountain belt: Central Range, Taiwan. *The Journal of Geology*, 108(1), 73-89. https://doi.org/10.1086/314387

Iverson, R.M. (2000). Landslide triggering by rain infiltration. *Water Resources Research*, 36(7), 1897-1910. https://doi.org/10.1029/2000WR900090

Jain, A.K., Kumar, D., Singh, S., Kumar, A., Lal, N. (2000). Timing, quantification and tectonic modelling of Pliocene–Quaternary movements in the NW Himalaya: evidence from fission track dating. *Earth and Planetary Science Letters*, 179(3-4), 437-451. https://doi.org/10.1016/S0012-821X(00)00133-3

Jones, D., Lister, D.H., Osborn, T.J., Harpham, C., Salmon, M., Morice, C. (2012). Hemispheric and large-scale land-surface air temperature variations: An extensive revision and an update to 2010. *Journal of Geophysical Research: Atmospheres*, 117(D5). https://doi.org/10.1029/2011JD017139

Kattel, D.B., Yao, T., Yang, K., Tian, L., Yang, G., Joswiak, D. (2013). Temperature lapse rate in complex mountain terrain on the southern slope of the central Himalayas. *Theoretical and applied climatology*, 113(3-4), 671-682. https://doi.org/10.1007/s00704-012-0816-6

Kohl, C., Nishiizumi, K. (1992). Chemical isolation of quartz for measurement of in situ produced cosmogenic nuclides. *Geochimica. Cosmochimica. Acta* 56, 3583–3587. https://doi.org/10.1016/0016-7037(92)90401-4

Kirchner, J.W., Finkel, R.C., Riebe, C.S., Granger, D.E., Clayton, J.L., King, J.G., Megahan, W.F., 2001. Mountain erosion over 10 yr, 10 ky, and 10 my time scales. *Geology*, 29(7), 591-594. https://doi.org/10.1130/0091-7613(2001)029<0591:MEOYKY>2.0.CO;2

Kirstein, L.A., Sinclair, H., Stuart, F.M., Dobson, K. (2006). Rapid early Miocene exhumation of the Ladakh batholith, western Himalaya. *Geology*, 34(12), 1049-1052. https://doi.org/10.1130/G22857A.1

Kirstein, L.A., Foeken, J.T., Van Der Beek, , Stuart, F.M., Phillips, R.J. (2009). Cenozoic unroofing history of the Ladakh Batholith, western Himalaya, constrained by thermochronology and numerical modelling. *Journal of the Geological Society*, 166(4), 667-678. https://doi.org/10.1144/0016-76492008-107

Kumar, A., Gupta, A.K., Bhambri, R., Verma, A., Tiwari, S.K., Asthana, A.K.L. (2018). Assessment and review of hydrometeorological aspects for cloudburst and flash flood events in the third pole region (Indian Himalaya). *Polar Science*. https://doi.org/10.1016/j.polar.2018.08.004

Lavé, J., Avouac, J. (2000). Active folding of fluvial terraces across the Siwaliks Hills, Himalayas of central Nepal. *Journal of Geophysical Research: Solid Earth*, 105(B3), 5735-5770. https://doi.org/10.1029/1999JB900292

Lavé, J., Avouac, J. (2001). Fluvial incision and tectonic uplift across the Himalayas of central Nepal. *Journal of Geophysical Research: Solid Earth*, 106(B11), 26561-26591. https://doi.org/10.1029/2001JB000359

Lal, D. (1991). Cosmic ray labelling of erosion surfaces: in situ nuclide production rates and erosion models. *Earth and Planetary Science Letters*,104, 429-439. https://doi.org/10.1016/0012-821X(91)90220-C

Lang, T.J., Barros, A. (2004). Winter storms in the central Himalayas. *Journal of the Meteorological Society of Japan*. Ser. II, 82(3), 829-844. https://doi.org/10.2151/jmsj.2004.829

Liu, X., Dong, B. (2013). Influence of the Tibetan Plateau uplift on the Asian monsoon-arid environment evolution. *Chinese Science Bulletin*, 58(34), 4277-4291. https://doi.org/10.1007/s11434-013-5987-8

Lukas S, Graf A, Coray S, Schlüchter C. (2012). Genesis, stability and preservation potential of large lateral moraines of Alpine valley glaciers–towards a unifying theory based on Findelengletscher, Switzerland. *Quaternary Science Reviews* 38: 27-48. https://doi.org/10.1016/j.quascirev.2012.01.022

Lupker M, Blard H, Lave J, France-Lanord C, Leanni L, Puchol N, Charreau J, Bourlès D. (2012). $^{10}$Be-derived Himalayan denudation rates and sediment budgets in the Ganga basin. *Earth and Planetary Science Letters* 333: 146-156. https://doi.org/10.1016/j.epsl.2012.04.020

MacGregor K.R, Anderson R.S, Waddington, E.D. (2009). Numerical modeling of glacial erosion and headwall processes in alpine valleys. *Geomorphology* 103(2): 189-204. https://doi.org/10.1016/j.geomorph.2008.04.022

Martin, L., Blard, , Balco, G., Laurent, V. (2017). The CREp program and the ICE-D production rate calibration database: A fully parameterizable and updated online tool to compute cosmic-ray exposure ages. *Quaternary Geochronology*, 38, 25-49. https://doi.org/10.1016/j.quageo.2016.11.006

Matsuoka N. (2001). Microgelivation versus macrogelivation: towards bridging the gap between laboratory and field frost weathering. *Permafrost and Periglacial Processes* 12(3): 299-313. https://doi.org/10.1002/ppp.393

Matsuoka N, Sakai H. (1999). Rockfall activity from an alpine cliff during thawing periods. *Geomorphology* 28(3-4): 309-328. https://doi.org/10.1016/S0169-555X(98)00116-0

Meunier, , Hovius, N., Haines, J.A. (2008). Topographic site effects and the location of earthquake induced landslides. *Earth and Planetary Science Letters*, 275(3-4), 221-232. https://doi.org/10.1016/j.epsl.2008.07.020

Miller, C., Klötzli, U., Frank, W., Thöni, M., Grasemann, B. (2000), Proterozoic crustal evolution in the NW Himalaya (India) as recorded by circa 1.80 Ga mafic and 1.84 Ga granitic magmatism: *Precambrian Research*, v. 103, 191–206. https://doi.org/10.1016/S0301-9268(00)00091-7

Miller, C., Thöni, M., Frank, W., Grasemann, B., Klötzli, U., Guntli, and Draganits, E. (2001). The early Palaeozoic magmatic event in the Northwest Himalaya, India: source, tectonic setting and age of emplacement. *Geological Magazine*, 138(3), 237-251. https://doi.org/10.1017/S0016756801005283

Mölg, T., Maussion, F.,Scherler, D. (2014). Mid-latitude westerlies as a driver of glacier variability in monsoonal High Asia. *Nature Climate Change*, 4(1), 68. https://doi.org/10.1038/nclimate2055

Moon, S., Perron, J.T., Martel, S.J., Holbrook, W.S., St. Clair, J., (2017). A model of three-dimensional topographic stresses with implications for bedrock fractures, surface processes, and landscape evolution. *Journal of Geophysical Research: Earth Surface*, 122(4), 823-846. https://doi.org/10.1002/2016JF004155

Moore, R.D., Fleming, S.W., Menounos, B., Wheate, R., Fountain, A., Stahl, K., Holm, K., Jakob, M. (2009). Glacier change in western North America: influences on hydrology, geomorphic hazards and water quality. *Hydrological Processes*, 23(1), 42-61. https://doi.org/10.1002/hyp.7162

Murari, M.K., Owen, L.A., Dortch, J.M., Caffee, M.W., Dietsch, C., Fuchs, M., Haneberg, W.C., Sharma, M.C., Townsend-Small, A. (2014). Timing and climatic drivers for glaciation across monsoon-influenced regions of the Himalayan–Tibetan orogen. *Quaternary Science Reviews*, 88, 159-182. https://doi.org/10.1016/j.quascirev.2014.01.013

Muzikar, P. (2008). Cosmogenic nuclide concentrations in episodically eroding surfaces: Theoretical results. *Geomorphology*, 97(3-4), 407-413. https://doi.org/10.1016/j.geomorph.2007.08.020

Nagai, H., Fujita, K., Nuimura, T., Sakai, A. (2013). Southwest-facing slopes control the formation of debris-covered glaciers in the Bhutan Himalaya. *The Cryosphere*, 7(4), 1303. https://doi.org/10.5194/tc-7-1303-2013

Naylor, S., Gabet, E.J. (2007). Valley asymmetry and glacial versus nonglacial erosion in the Bitterroot Range, Montana, USA. *Geology*, 35(4), 375-378. https://doi.org/10.1130/G23283A.1

Nishiizumi, K., Winterer, E.L., Kohl, C.P., Klein, J., Middleton, R., Lal, D., Arnold, J.R. (1989). Cosmic ray production rates of $^{10}$Be and $^{26}$Al in quartz from glacially polished rocks. *Journal of Geophysical Research: Solid Earth*, 94(B12), 17907-17915. https://doi.org/10.1029/JB094iB12p17907

Orr, E., Owen, L., Murari, M., Saha, S., Caffee, M. (2017). The timing and extent of Quaternary glaciation of Stok, northern Zanskar Range, Transhimalaya, of northern India. *Geomorphology* 284, 142-155. https://doi.org/10.1016/j.geomorph.2016.05.031

Orr, E.N., Owen, L.A., Saha, S., Caffee, M.W., Murari, M.K. (2018). Quaternary glaciation of the Lato Massif, Zanskar Range of the NW Himalaya. *Quaternary Science Reviews*, 183, 140-156. https://doi.org/10.1016/j.quascirev.2018.01.005

Orr, E.N., Owen, L.A., Saha, S., Caffee, M.W. (2019). Rates of rockwall slope erosion in the upper Bhagirathi catchment, Garhwal Himalaya. *Earth Surface Processes and Landforms*, 44(15),3108-3127, https://doi.org/10.1002/esp.4720

Osborn, T.J., Jones, P. (2014). The CRUTEM4 land-surface air temperature data set: construction, previous versions and dissemination via Google Earth. Earth System Science Data, 6(1), 61-68. https://doi.org/10.5194/essd-6-61-2014

Osmaston, H. (2005). Estimates of glacier equilibrium line altitudes by the Area× Altitude, the Area× Altitude Balance Ratio and the Area× Altitude Balance Index methods and their validation. Quaternary International 138: 22-31. https://doi.org/10.1016/j.quaint.2005.02.004

Oskin, M., Burbank, D.W. (2005). Alpine landscape evolution dominated by cirque retreat. *Geology* 33(12): 933-936. https://doi.org/10.1130/G21957.1

Ouimet, W.B., Whipple, K.X., Granger, D.E. (2009). Beyond threshold hillslopes: Channel adjustment to base-level fall in tectonically active mountain ranges. *Geology* 37(7): 579-582. https://doi.org/10.1130/G30013A.1

Owen, L., Dortch, J. (2014). Nature and timing of Quaternary glaciation in the Himalayan-Tibetan orogen. *Quaternary Science Reviews* 88, 14-54. https://doi.org/10.1016/j.quascirev.2013.11.016

Owen, L.A., Sharma, M.C. (1998). Rates and magnitudes of paraglacial fan formation in the Garhwal Himalaya: implications for landscape evolution. *Geomorphology*, 26(1-3), 171-184. https://doi.org/10.1016/S0169-555X(98)00057-9

Owen, L.A., Derbyshire E, Scott C.H. (2003). Contemporary sediment production and transfer in high-altitude glaciers. *Sedimentary Geology* 155(1-2): 13-36. https://doi.org/10.1016/S0037-0738(02)00156-2

Owen, L., Caffee, M., Bovard, K., Finkel, R., Sharma, M. (2006). Terrestrial cosmogenic nuclide surface exposure dating of the oldest glacial successions in the Himalayan orogen: Ladakh Range, northern India. *GSA Bulletin*, 118, 3-4, 383-392. https://doi.org/10.1130/B25750.1

Owen, L.A., Caffee, M.W., Finkel, R.C., Seong, B.S. (2008). Quaternary glaciation of the Himalayan–Tibetan orogen. *Journal of Quaternary Science*, 23, 513–532. https://doi.org/10.1002/jqs.1203

Patel, L.K., Sharma, P., Fathima, T.N., Thamban, M. (2018). Geospatial observations of topographical control over the glacier retreat, Miyar basin, Western Himalaya, India. *Environmental Earth Sciences*, *77*(5), 190. https://doi.org/10.1007/s12665-018-7379-5

Portenga E.W, Bierman, R. (2011). Understanding Earth's eroding surface with $^{10}$Be. *GSA Today* 21(8): 4-10.

Portenga E.W, Bierman R, Duncan C, Corbett L.B, Kehrwald N.M, Rood, D.H. (2015). Erosion rates of the Bhutanese Himalaya determined using in situ-produced $^{10}$Be. *Geomorphology* 233: 112-126. https://doi.org/10.1016/j.geomorph.2014.09.027

Pratap, B., Dobhal, D., Bhambri, R., Mehta, M. (2013). Near-surface temperature lapse rate in Dokriani Glacier catchment, Garhwal Himalaya, India. *Himalayan Geology*, 34, 183-186.

Qiang, X.K., Li, Z.X., Powell, C.M., Zheng, H.B. (2001). Magnetostratigraphic record of the Late Miocene onset of the East Asian monsoon, and Pliocene uplift of northern Tibet. *Earth and*

*Planetary Science Letters*,187, 1-2, 83-93. https://doi.org/10.1016/S0012-821X(01)00281-3

Rajendran, K., Rajendran, C., Jain, S.K., Murty, C.V.R.,Arlekar, J.N. (2000). The Chamoli earthquake, Garhwal Himalaya: field observations and implications for seismic hazard. *Current Science*, 78(1), 45-51.

Regmi, D., Watanabe, T. (2009). Rockfall activity in the Kangchenjunga area, Nepal Himalaya. *Permafrost and Periglacial Processes*, 20(4), 390-398. https://doi.org/10.1002/ppp.664

Robert, X., Van Der Beek, , Braun, J., Perry, C., Mugnier, J.L. (2011). Control of detachment geometry on lateral variations in exhumation rates in the Himalaya: Insights from low-temperature thermochronology and numerical modeling. *Journal of Geophysical Research: Solid Earth*, 116(B5). https://doi.org/10.1029/2010JB007893

Sadler M, Jerolmack, D.J. (2014). Scaling laws for aggradation, denudation and progradation rates: the case for time-scale invariance at sediment sources and sinks. *Geological Society, London, Special Publications* 404: 404-7. https://doi.org/10.1144/SP404.7

Saha, S., Owen, L.A., Orr, E.N., Caffee, M.W. (2018). Timing and nature of Holocene glacier advances at the northwestern end of the Himalayan-Tibetan orogen. *Quaternary Science Reviews*, 187, 177-202. https://doi.org/10.1016/j.quascirev.2018.03.009

Saha, S., Owen, L.A., Orr, E.N., Caffee, M.W. (2019). High-frequency Holocene glacier fluctuations in the Himalayan-Tibetan orogen. *Quaternary Science Reviews*, 220, 372-400. https://doi.org/10.1016/j.quascirev.2019.07.021

Sagredo, E.A., Lowell, T.V. (2012). Climatology of Andean glaciers: A framework to understand glacier response to climate change. *Global and Planetary Change*, 86, 101-109. https://doi.org/10.1016/j.gloplacha.2012.02.010

Sanders, J.W., Cuffey, K.M., Moore, J.R., MacGregor, K.R. and Kavanaugh, J.L. (2012). Periglacial weathering and headwall erosion in cirque glacier bergschrunds. *Geology*, 40(9), 779-782. https://doi.org/10.1130/G33330.1

Sanders, J.W., Cuffey, K.M., MacGregor, K.R. and Collins, B.D. (2013). The sediment budget of an alpine cirque. *GSA Bulletin*, 125(1-2), 229-248. https://doi.org/10.1130/B30688.1

Sarr, A.C., Mugnier, J.L., Abrahami, R., Carcaillet, J., Ravanel, L., (2019). Sidewall erosion: Insights from in situ-produced $^{10}$Be concentrations measured on supraglacial clasts (Mont Blanc massif, France). *Earth Surface Processes and Landforms*, 44(10),1930-1944. https://doi.org/10.1002/esp.4620

Schelling, D., Arita, K. (1991). Thrust tectonics, crustal shortening, and the structure of the far-eastern Nepal Himalaya. *Tectonics*, 10(5), 851-862. https://doi.org/10.1029/91TC01011

Scherler D, Bookhagen B, Strecker M.R. (2011). Hillslope-glacier coupling: The interplay of topography and glacial dynamics in High Asia. *Journal of Geophysical Research: Earth Surface*: 116(F2). https://doi.org/10.1029/2010JF001751

Scherler, D., Bookhagen, B., Strecker, M.R. (2014). Tectonic control on $^{10}$Be-derived erosion rates in the Garhwal Himalaya, India. *Journal of Geophysical Research: Earth Surface*, 119(2), 83-105. https://doi.org/10.1002/2013JF002955

Scherler, D., Bookhagen, B., Wulf, H., Preusser, F., Strecker, M.R. (2015). Increased late Pleistocene erosion rates during fluvial aggradation in the Garhwal Himalaya, northern India. *Earth and Planetary Science Letters*, 428, 255-266. https://doi.org/10.1016/j.epsl.2015.06.034

Scherler, D., Egholm, D. (2017). Debris supply to mountain glaciers and how it effects their sensitivity to climate change–A case study from the Chhota Shigri Shigri Glacier, India (Invited)(206444). In 2017 Fall Meeting.

Schlup, M., Carter, A., Cosca, M., Steck, A. (2003). Exhumation history of eastern Ladakh revealed by 40Ar/39Ar and fission-track ages: the Indus River- Tso Morari transect, NW Himalayas. *Journal of the Geological Society*, 160, 385-399. https://doi.org/10.1144/0016-764902-084

Schlup, M., Steck, A., Carter, A., Cosca, M., Epard, J.L., Hunziker, J. (2011). Exhumation history of the NW Indian Himalaya revealed by fission track and 40Ar/39Ar ages. *Journal of Asian Earth Sciences*, *40*(1), 334-350. https://doi.org/10.1016/j.jseaes.2010.06.008

Schroder J.F, Bishop M.P, Copland L, Sloan V.F. (2000). Debris-covered glaciers and rock glaciers in the Nanga Parbat Himalaya, Pakistan. *Geografiska Annaler*: Series A, 82A, 17–31. https://doi.org/10.1111/j.0435-3676.2000.00108.x

Seaby, R., Henderson, P. (2014)."Community Analysis Package 5.0."

Searle, M. (1986). Structural evolution and sequence of thrusting in the High Himalayan, Tibetan-Tethys and Indus suture zones of Zanskar and Ladakh, Western Himalaya. *Journal of Structural Geology*, 8,8, 923-936. https://doi.org/10.1016/0191-8141(86)90037-4

Searle, M., Fryer, B.J. (1986). Garnet, tourmaline and muscovite-bearing leucogranites, gneisses and migmatites of the Higher Himalayas from Zanskar, Kulu, Lahoul and Kashmir. *Geological Society, London, Special Publications*, 19(1), 185-201. https://doi.org/10.1144/GSL.SP.1986.019.01.10

Searle M.P, Noble S.R, Hurford A.J, Rex, D.C. (1999). Age of crustal melting, emplacement and exhumation history of the Shivling leucogranite, Garhwal Himalaya. *Geological Magazine* 136(5): 513 525. https://doi.org/10.1017/S0016756899002885

Searle, M., Parrish, R., Hodges, K., Hurford, A., Ayres, M., Whitehouse, M. (1997). Shisha Pangma Leucogranite, South Tibetan Himalaya: Field Relations, Geochemistry, Age, Origin, and Emplacement. *Journal of Geology*, 150, 295-317. https://doi.org/10.1086/515924

Searle, M.P., Elliott, J.R., Phillips, R.J., Chung, S.L. (2011). Crustal–lithospheric structure and continental extrusion of Tibet. *Journal of the Geological Society*, 168(3), 633-672. https://doi.org/10.1144/0016-76492010-139

Seong Y.B, Owen L.A, Caffee M.W, Kamp U, Bishop M.P, Bush A, Copland L, Shroder, J.F. (2009). Rates of basin-wide rockwall retreat in the K2 region of the Central Karakoram defined by terrestrial cosmogenic nuclide $^{10}$Be. *Geomorphology* 107(3-4): 254-262. https://doi.org/10.1016/j.geomorph.2008.12.014

Sharma, P., Bourgeois, M., Elmore, D., Granger, D., Lipschutz, M.E., Ma, X., Miller, T., Mueller, K., Rickey, F., Simms,P, Vogt, S. (2000) PRIME lab AMS performance, upgrades and research applications. *Nuclear Instruments and Methods in Physics Research*, B 172, 112-123. https://doi.org/10.1016/S0168-583X(00)00132-4

Sharma, S., Shukla, A.D., Bartarya, S.K., Marh, B.S., Juyal, N. (2017). The Holocene floods and their affinity to climatic variability in the western Himalaya, India. *Geomorphology*, *290*, 317-334. https://doi.org/10.1016/j.geomorph.2017.04.030

Small, R.J. (1983). Lateral moraines of Glacier de Tsidjiore Nouve: form, development, and implications. *Journal of Glaciology* 29(102): 250-259. https://doi.org/10.3189/S0022143000008303

Small, E.E., Anderson, R.S. (1998). Pleistocene relief production in Laramide mountain ranges, western United States. *Geology*, 26(2), 123-126. https://doi.org/10.1130/0091-7613(1998)026<0123:PRPILM>2.3.CO;2

Small, E.E., Anderson, R.S., Repka, J.L., Finkel, R. (1997). Erosion rates of alpine bedrock summit surfaces deduced from in situ $^{10}$Be and $^{26}$Al. *Earth and Planetary Science Letters*, 150(3-4), 413-425. https://doi.org/10.1016/S0012-821X(97)00092-7

Solomina, O.N., Bradley, R.S., Hodgson, D.A., Ivy-Ochs, S., Jomelli, V., Mackintosh, A.N., Nesje, A., Owen, L.A., Wanner, H., Wiles, G.C., Young, N.E. (2015). Holocene glacier fluctuations. *Quaternary Science Reviews*, 111, 9-34. https://doi.org/10.1016/j.quascirev.2014.11.018

Solomina, O.N., Bradley, R.S., Jomelli, V., Geirsdottir, A., Kaufman, D.S., Koch, J., McKay, N., Masiokas, M., Miller, G., Nesje, A., Nicolussi, K. (2016). Glacier fluctuations during the past 2000 years. *Quaternary Science Reviews*, 149, 61-90. https://doi.org/10.1016/j.quascirev.2016.04.008

Sorkhabi, R.B., Stump, E., Foland, K.A., Jain, A.K. (1996). Fission-track and $^{40}$Ar$^{39}$Ar evidence for episodic denudation of the Gangotri granites in the Garhwal Higher Himalaya, India. *Tectonophysics*, 260(1-3), 187-199. https://doi.org/10.1016/0040-1951(96)00083-2

Sorkhabi, R.B., Stump, E., Foland, K., Jain, A.K. (1999). Tectonic and cooling history of the Garhwal Higher Himalaya (Bhagirathi Valley): constraints from thermochronological data. Geodynamics of the NW Himalaya. *Gondwana Research Group Memoir*, 6, 217-235.

Srivastava, P., Mitra, G. (1994). Thrust geometries and deep structure of the outer and lesser Himalaya, Kumaon and Garhwal (India): Implications for evolution of the Himalayan fold-and-thrust belt. *Tectonics*, 13(1), 89-109. https://doi.org/10.1029/93TC01130

Strahler, A.N. (1952). Hypsometric (area-altitude) analysis of erosional topography. *Geological Society of America Bulletin*, 63(11), 1117-1142. https://doi.org/10.1130/0016-7606(1952)63[1117:HAAOET]2.0.CO;2

Steck, A., Epard, J., Vannay, J., Hunziker, J., Girard, M., Morard, A., Robyr, M. (1998). Geological transect across the Tso Morari and Spiti areas- the nappe structures of the Tethys Himalayas. *Eclogae Geologicae Helvetiae* 91, 103-121.

Streule, M.J., Searle, M., Waters, D.J., Horstwood, M.S. (2010). Metamorphism, melting, and channel flow in the Greater Himalayan Sequence and Makalu leucogranite: Constraints from thermobarometry, metamorphic modeling, and U-Pb geochronology. *Tectonics*. 29, 5. https://doi.org/10.1029/2009TC002533

Su, Z., Shi, Y. (2002). Response of monsoonal temperate glaciers to global warming since the Little Ice Age. *Quaternary International*, 97, 123-131. https://doi.org/10.1016/S1040-6182(02)00057-5

Thayyen, R.J., Gergan, J.T., Dobhal, D. (2005). Slope lapse rates of temperature in Din Gad (Dokriani glacier) catchment, Garhwal Himalaya, India. *Bulletin of Glaciological Research*, 22, 31-37.

Thiede, R.C., Bookhagen, B., Arrowsmith, J.R., Sobel, E.R., Strecker, M.R. (2004). Climatic control on rapid exhumation along the Southern Himalayan Front. *Earth and Planetary Science Letters*, 222(3-4), 791-806. https://doi.org/10.1016/j.epsl.2004.03.015

Thiede, R.C., Arrowsmith, J.R., Bookhagen, B., McWilliams, M.O., Sobel, E.R., Strecker, M.R. (2005). From tectonically to erosionally controlled development of the Himalayan orogen. *Geology*, 33(8), 689-692. https://doi.org/10.1130/G21483AR.1

Thiede, R.C., Arrowsmith, J.R., Bookhagen, B., McWilliams, M., Sobel, E.R., Strecker, M.R. (2006). Dome formation and extension in the Tethyan Himalaya, Leo Pargil, northwest India. *Geological Society of America Bulletin*, 118(5-6), 635-650. https://doi.org/10.1130/B25872.1

Thiede, R.C., Ehlers, T.A., Bookhagen, B., Strecker, M.R. (2009). Erosional variability along the northwest Himalaya. *Journal of Geophysical Research: Earth Surface*, 114(F1). https://doi.org/10.1029/2008JF001010

Thiede, R.C., Ehlers, T.A. (2013). Large spatial and temporal variations in Himalayan denudation. *Earth and Planetary Science Letters*, 371, 278-293. https://doi.org/10.1016/j.epsl.2013.03.004

Thomas, E.K., Huang, Y., Clemens, S.C., Colman, S.M., Morrill, C., Wegener, , Zhao, J. (2016). Changes in dominant moisture sources and the consequences for hydroclimate on the northeastern Tibetan Plateau during the past 32 kyr. *Quaternary Science Reviews*, 131, 157-167. https://doi.org/10.1016/j.quascirev.2015.11.003

Thompson, L.O., Yao, T., Davis, M.E., Henderson, K.A., Mosley-Thompson, E., Lin, N., Beer, J., Synal, H.A., Cole-Dai, J., Bolzan, J.F. (1997). Tropical climate instability: The last glacial cycle from a Qinghai-Tibetan ice core. *Science*, 276(5320), 1821-1825. https://doi.org/10.1126/science.276.5320.1821

Upreti, B. (1999). An overview of the stratigraphy and tectonics of the Nepal Himalaya. *Journal of Asian Earth Science,* 17, 5-6, 577-606. https://doi.org/10.1016/S1367-9120(99)00047-4

Valdiya, K.S. (1991). The Uttarkashi earthquake of 20 October: implications and lessons. *Current Science* 61: 801–803. http://pascal-francis.inist.fr/vibad/index.php?action=getRecordDetail&idt=5222562

Vance, D, Bickle, M, Ivy-Ochs, S., Kubik, W. (2003). Erosion and exhumation in the Himalaya from cosmogenic isotope inventories of river sediments. *Earth and Planetary Science Letters*, 206(3-4), 273-288. https://doi.org/10.1016/S0012-821X(02)01102-0

Van Der Beek, , Van Melle, J., Guillot, S., Pêcher, A., Reiners, W., Nicolescu, S., Latif, M. (2009). Eocene Tibetan plateau remnants preserved in the northwest Himalaya. *Nature Geoscience*, 2(5), 364. https://doi.org/10.1038/ngeo503

Von Blanckenburg, F., Hewawasam, T.,Kubik, P.W. (2004). Cosmogenic nuclide evidence for low weathering and denudation in the wet, tropical highlands of Sri Lanka. *Journal of Geophysical Research: Earth Surface*, 109(F3). https://doi.org/10.1029/2003JF000049

Vannay, C., Grasemann, B., Rahn, M., Frank, W., Carter, A., Baudraz, V., Cosca, M. (2004). Miocene to Holocene exhumation of metamorphic crustal wedges in the NW Himalaya: Evidence for tectonic extrusion coupled to fluvial erosion. *Tectonics*, 23, 1-24. https://doi.org/10.1029/2002TC001429

Walia, M., Yang, T.F., Liu, T.K., Kumar, R., Chung, L. (2008). Fission track dates of Mandi granite and adjacent tectonic units in Kulu–Beas valley, NW Himalaya, India. *Radiation Measurements*, 43, S343-S347. https://doi.org/10.1016/j.radmeas.2008.04.040

Walker, J.D., Martin, M.W., Bowring, S.A., Searle, M., Waters, D.J., Hodges, K.V. (1999). Metamorphism, melting, and extension: Age constraints from the High Himalayan slab of southeast Zanskar and northwest Lahaul. *The Journal of Geology*, 107(4), 473-495. https://doi.org/10.1086/314360

Ward, D.J., Anderson, R.S. (2011). The use of ablation-dominated medial moraines as samplers for $^{10}$Be-derived erosion rates of glacier valley walls, Kichatna Mountains, AK. *Earth Surface Processes and Landforms* 36(4): 495-512. https://doi.org/10.1002/esp.2068

Watanabe, T., Dali, L., Shiraiwa, T. (1998). Slope denudation and the supply of debris to cones in Langtang Himal, Central Nepal Himalaya. *Geomorphology*, 26(1-3), 185-197. https://doi.org/10.1016/S0169-555X(98)00058-0

Weiers, S. (1995). On the climatology of the NW Karakorum and adjacent areas: Statistical analyzes including weather satellite images and a Geographical Information System (GIS). In commission with F. Dümmler.

Willenbring, J.K., Gasparini, N.M., Crosby, B.T., Brocard, G. (2013). What does a mean mean? The temporal evolution of detrital cosmogenic denudation rates in a transient landscape. *Geology*, 41(12), 1215-1218. https://doi.org/10.1130/G34746.1

Wittmann, H., Malusà, M.G., Resentini, A., Garzanti, E., Niedermann, S. (2016). The cosmogenic record of mountain erosion transmitted across a foreland basin: Source-to-sink analysis of in situ 10Be, 26Al and 21Ne in sediment of the Po river catchment. *Earth and Planetary Science Letters*, *452*, 258-271. https://doi.org/10.1016/j.epsl.2016.07.017

Wobus, C.W., Hodges, K.V.,Whipple, K.X. (2003). Has focused denudation sustained active thrusting at the Himalayan topographic front? *Geology*, 31(10), 861-864. https://doi.org/10.1130/G19730.1

Wulf, H., Bookhagen, B., Scherler, D. (2010). Seasonal precipitation gradients and their impact on fluvial sediment flux in the Northwest Himalaya. *Geomorphology*, 118, 1-2, 13-21. https://doi.org/10.1016/j.geomorph.2009.12.003

Yanites, B.J., Tucker, G.E., Anderson, R.S. (2009). Numerical and analytical models of cosmogenic radionuclide dynamics in landslide-dominated drainage basins. *Journal of Geophysical Research: Earth Surface,* 114(F1). https://doi.org/10.1029/2008JF001088

Yin, A., Harrison, T.M. (2000). Geologic evolution of the Himalayan-Tibetan orogen. *Annual Review of Earth and Planetary Science*, 28, 1, 211-280.

Zeitler, K., Koons, O., Bishop, M., Chamberlain, C., Craw, D., Edwards, M.A., Hamidullah, S., Jan, M.Q., Khan, M.A., Khattak, M., Kidd, W.S. (2001). Crustal reworking at Nanga Parbat, Pakistan: Metamorphic consequences of thermal-mechanical coupling facilitated by erosion. Tectonics, 20(5), 712-728. https://doi.org/10.1029/2000TC001243

**Figure_1.**

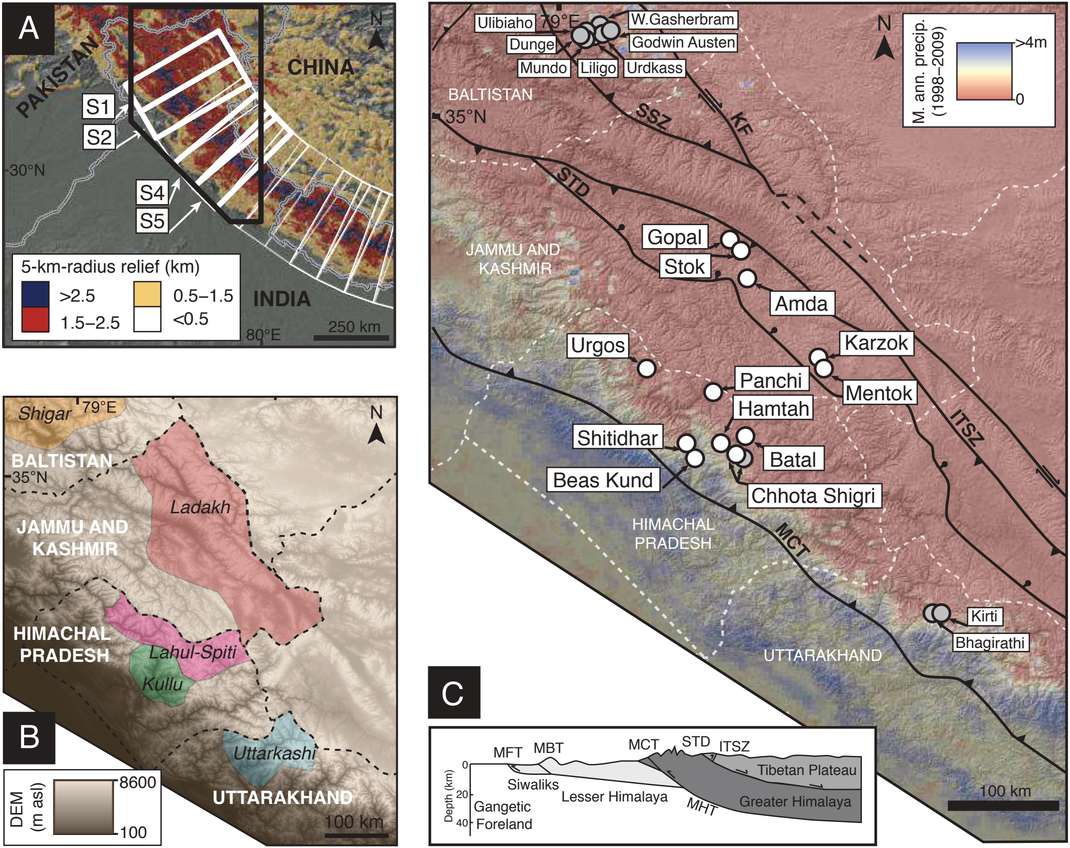
A
PAKISTAN
CHINA
INDIA
N
S1
S2
S4
S5
30°N
80°E
250 km
5-km-radius relief (km)
>2.5
1.5–2.5
0.5–1.5
<0.5
B
Shigar
79°E
BALTISTAN
35°N
JAMMU AND KASHMIR
Ladakh
HIMACHAL PRADESH
Lahul-Spiti
Kullu
Uttarkashi
UTTARAKHAND
100 km
DEM (m asl)
8600
100
Ulibiaho
79°E
W.Gasherbram
Dunge
Godwin Austen
Mundo
Liligo
Urdkass
BALTISTAN
35°N
SSZ
KF
STD
M. ann. precip. (1998–2009)
>4m
0
JAMMU AND KASHMIR
Gopal
Stok
Amda
Karzok
Urgos
Panchi
Mentok
Hamtah
ITSZ
Shitidhar
Batal
Beas Kund
Chhota Shigri
HIMACHAL PRADESH
MCT
Kirti
Bhagirathi
UTTARAKHAND
C
MFT
MBT
MCT
STD
ITSZ
Depth (km)
0
20
40
Siwaliks
Lesser Himalaya
Tibetan Plateau
Gangetic Foreland
MHT
Greater Himalaya
100 km

**Figure_2.**

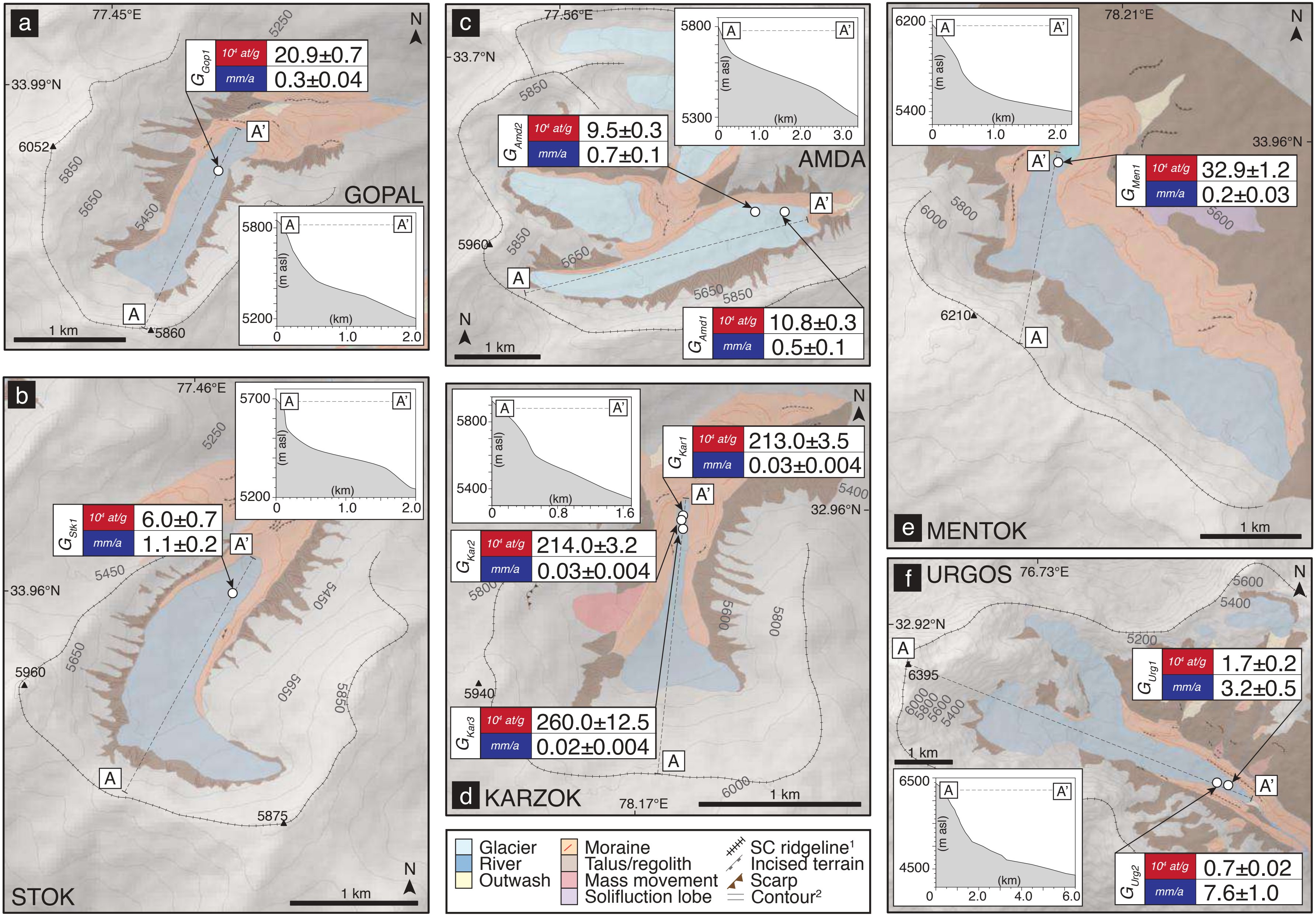

a
77.45°E
33.99°N
N
$G_{Gop1}$
$10^4$ at/g 20.9±0.7
mm/a 0.3±0.04
GOPAL
6052
5860
A
A'
1 km
5800 5200 (m asl) 0 1.0 2.0 (km)
b
77.46°E
33.96°N
$G_{Stk1}$
$10^4$ at/g 6.0±0.7
mm/a 1.1±0.2
STOK
5960
5875
5700 5200 (m asl) 0 1.0 2.0 (km)
1 km
c
77.56°E
33.7°N
AMDA
$G_{Amd2}$
$10^4$ at/g 9.5±0.3
mm/a 0.7±0.1
$G_{Amd1}$
$10^4$ at/g 10.8±0.3
mm/a 0.5±0.1
5960
5800 5300 (m asl) 0 1.0 2.0 3.0 (km)
1 km
d KARZOK
78.17°E
32.96°N
$G_{Kar1}$
$10^4$ at/g 213.0±3.5
mm/a 0.03±0.004
$G_{Kar2}$
$10^4$ at/g 214.0±3.2
mm/a 0.03±0.004
$G_{Kar3}$
$10^4$ at/g 260.0±12.5
mm/a 0.02±0.004
5940
5800 5400 (m asl) 0 0.8 1.6 (km)
1 km
e MENTOK
78.21°E
33.96°N
$G_{Men1}$
$10^4$ at/g 32.9±1.2
mm/a 0.2±0.03
6210
6200 5400 (m asl) 0 1.0 2.0 (km)
1 km
f URGOS
76.73°E
32.92°N
6395
$G_{Urg1}$
$10^4$ at/g 1.7±0.2
mm/a 3.2±0.5
$G_{Urg2}$
$10^4$ at/g 0.7±0.02
mm/a 7.6±1.0
6500 4500 (m asl) 0 2.0 4.0 6.0 (km)
1 km
Glacier
River
Outwash
Moraine
Talus/regolith
Mass movement
Solifluction lobe
SC ridgeline[1]
Incised terrain
Scarp
Contour[2]

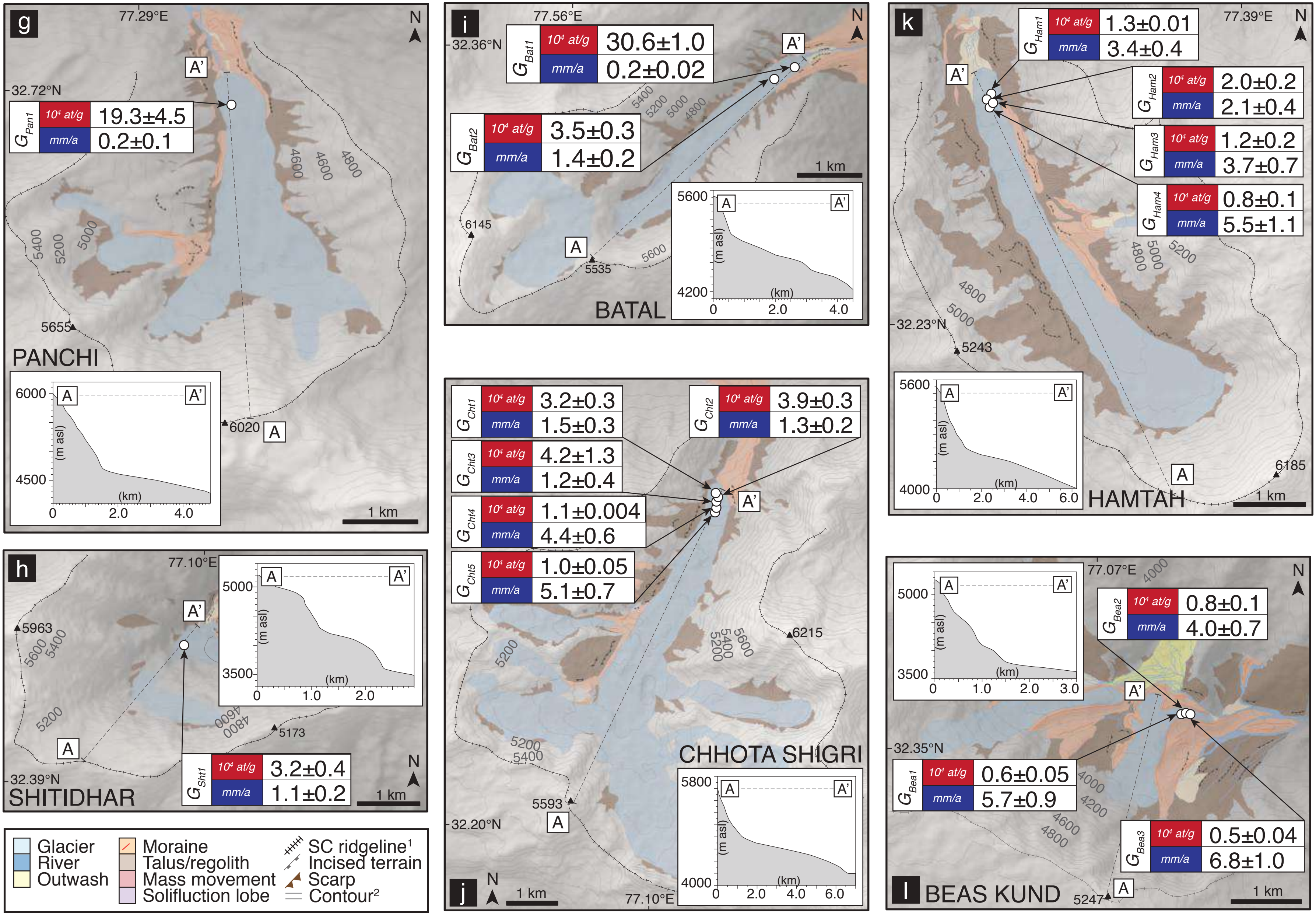

g
PANCHI
77.29°E
32.72°N
$G_{Pan1}$ 10⁴ at/g 19.3±4.5 mm/a 0.2±0.1
h
SHITIDHAR
77.10°E
32.39°N
$G_{Sht1}$ 10⁴ at/g 3.2±0.4 mm/a 1.1±0.2
i
BATAL
77.56°E
32.36°N
$G_{Bat1}$ 10⁴ at/g 30.6±1.0 mm/a 0.2±0.02
$G_{Bat2}$ 10⁴ at/g 3.5±0.3 mm/a 1.4±0.2
j
CHHOTA SHIGRI
32.20°N
77.10°E
$G_{Cht1}$ 10⁴ at/g 3.2±0.3 mm/a 1.5±0.3
$G_{Cht2}$ 10⁴ at/g 3.9±0.3 mm/a 1.3±0.2
$G_{Cht3}$ 10⁴ at/g 4.2±1.3 mm/a 1.2±0.4
$G_{Cht4}$ 10⁴ at/g 1.1±0.004 mm/a 4.4±0.6
$G_{Cht5}$ 10⁴ at/g 1.0±0.05 mm/a 5.1±0.7
k
HAMTAH
77.39°E
32.23°N
$G_{Ham1}$ 10⁴ at/g 1.3±0.01 mm/a 3.4±0.4
$G_{Ham2}$ 10⁴ at/g 2.0±0.2 mm/a 2.1±0.4
$G_{Ham3}$ 10⁴ at/g 1.2±0.2 mm/a 3.7±0.7
$G_{Ham4}$ 10⁴ at/g 0.8±0.1 mm/a 5.5±1.1
l
BEAS KUND
77.07°E
32.35°N
$G_{Bea1}$ 10⁴ at/g 0.6±0.05 mm/a 5.7±0.9
$G_{Bea2}$ 10⁴ at/g 0.8±0.1 mm/a 4.0±0.7
$G_{Bea3}$ 10⁴ at/g 0.5±0.04 mm/a 6.8±1.0
(m asl)
(km)
1 km
Glacier
River
Outwash
Moraine
Talus/regolith
Mass movement
Solifluction lobe
SC ridgeline[1]
Incised terrain
Scarp
Contour[2]

**Figure_3.**


A
B
C
D
E
F

**Figure_4.**

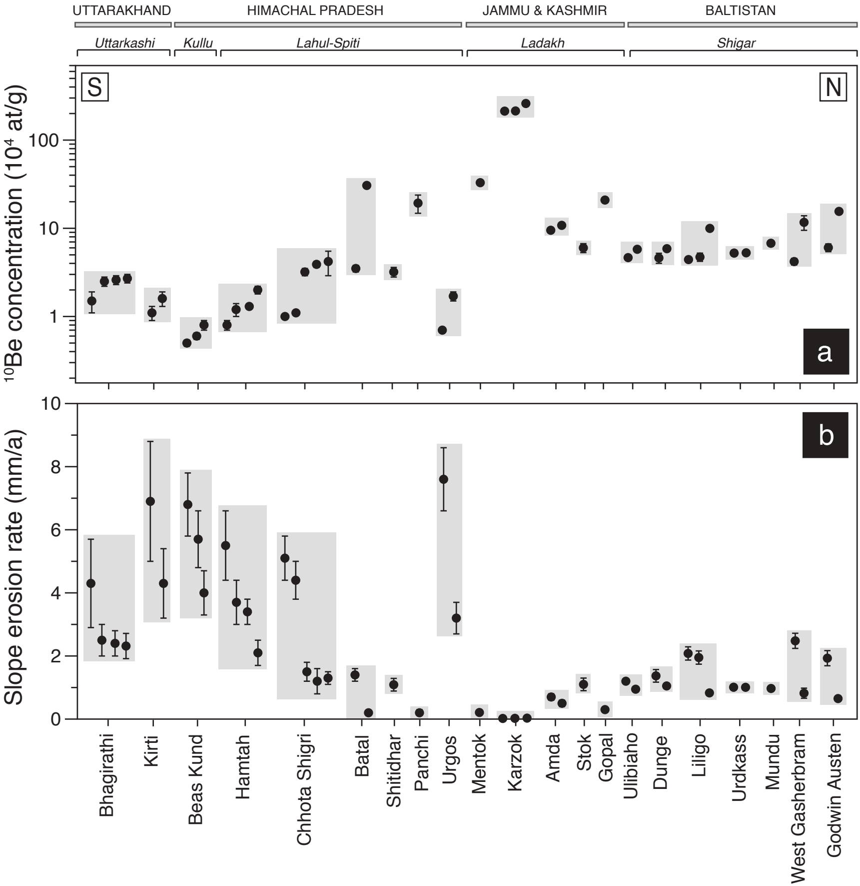

UTTARAKHAND
HIMACHAL PRADESH
JAMMU & KASHMIR
BALTISTAN
Uttarkashi
Kullu
Lahul-Spiti
Ladakh
Shigar
S
N
$^{10}$Be concentration ($10^4$ at/g)
100
10
1
a
Slope erosion rate (mm/a)
10
8
6
4
2
0
b
Bhagirathi
Kirti
Beas Kund
Hamtah
Chhota Shigri
Batal
Shitidhar
Panchi
Urgos
Mentok
Karzok
Amda
Stok
Gopal
Ulibiaho
Dunge
Liligo
Urdkass
Mundu
West Gasherbram
Godwin Austen

Figure_5.

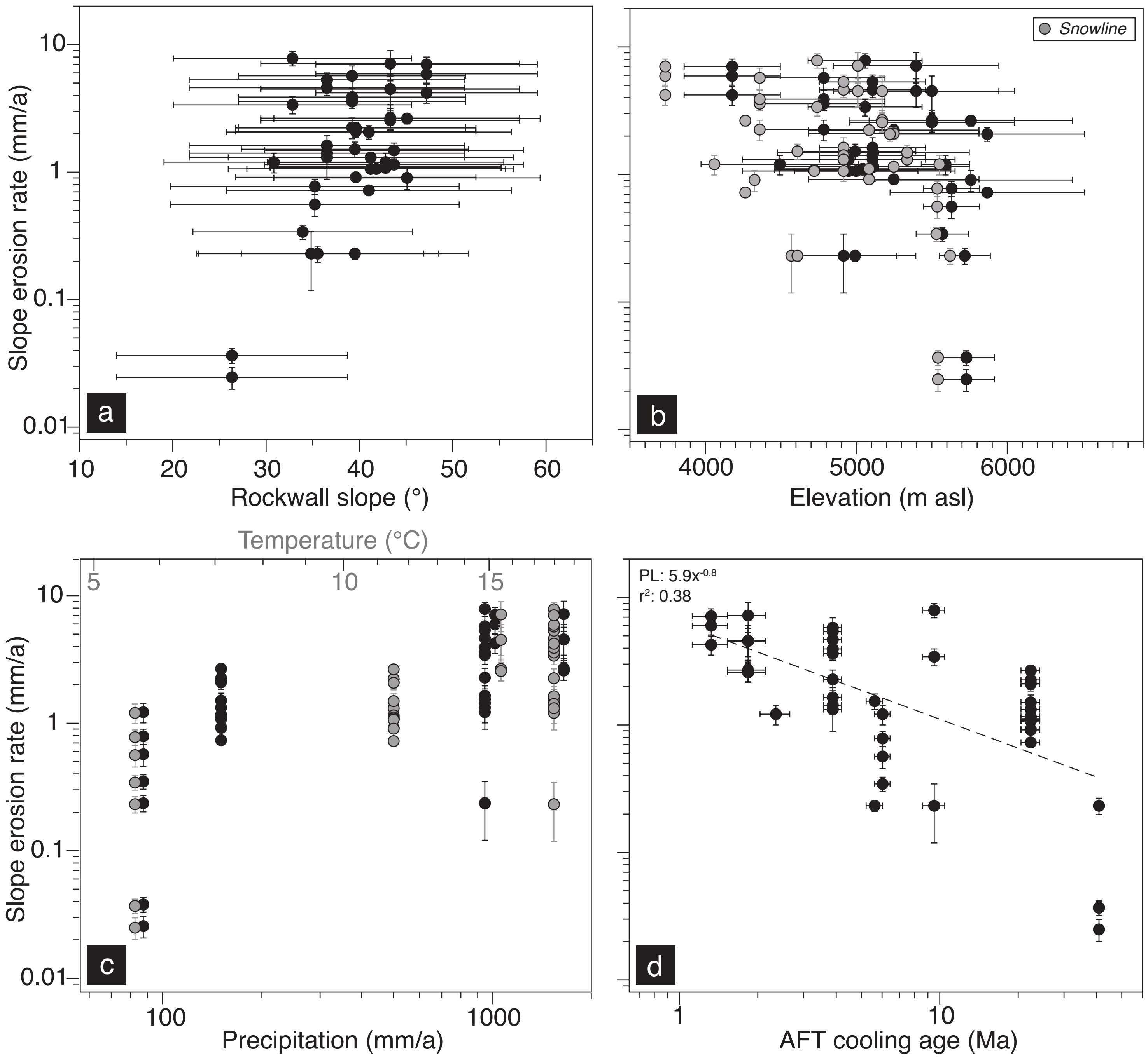

Slope erosion rate (mm/a)
10
1
0.1
0.01
a
10
20
30
40
50
60
Rockwall slope (°)
Snowline
b
4000
5000
6000
Elevation (m asl)
Temperature (°C)
5
10
15
c
100
1000
Precipitation (mm/a)
PL: 5.9x^-0.8
r^2: 0.38
d
1
10
AFT cooling age (Ma)

**Figure_6.**

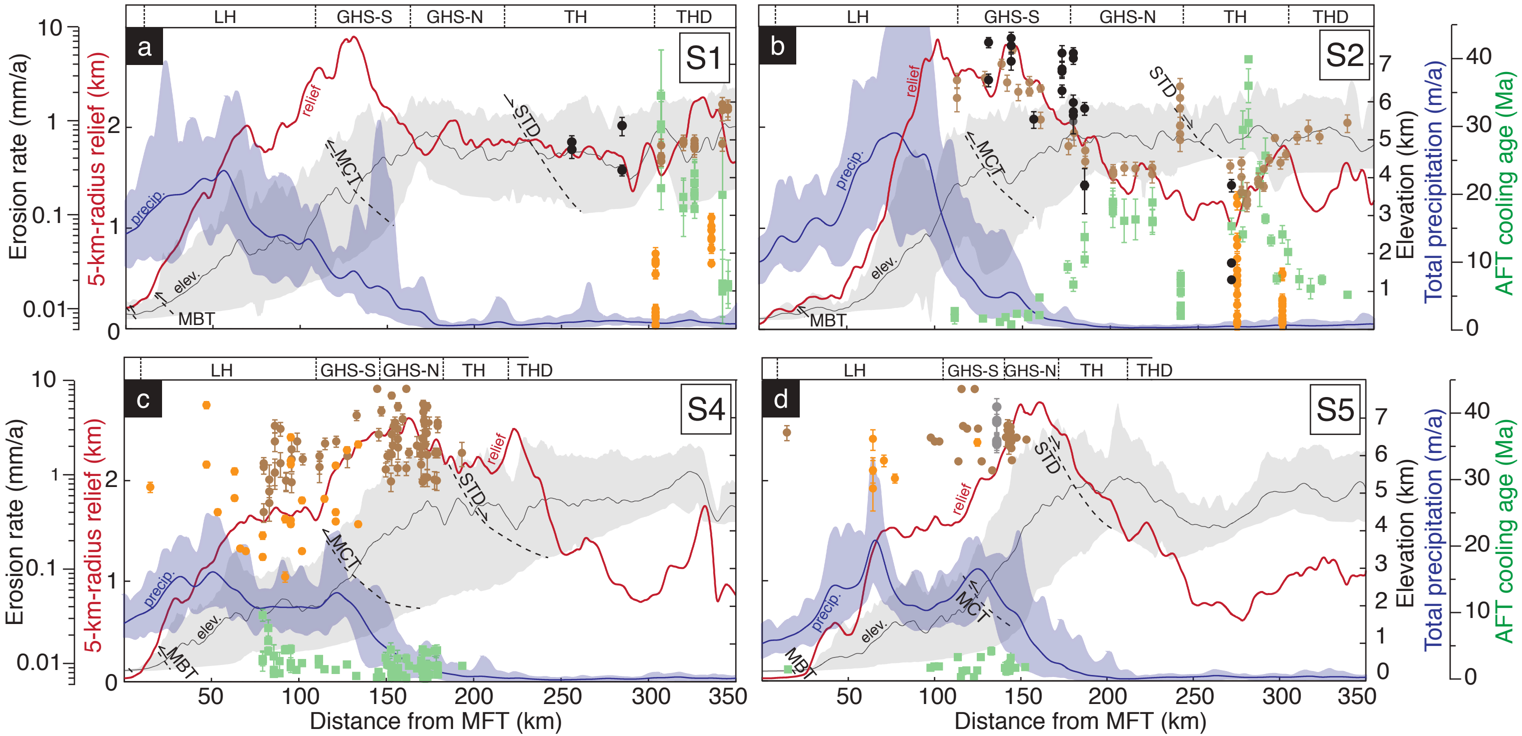


● Rockwall slope erosion *(this study)* ● Rockwall slope erosion ● Catchment-wide erosion ■ AFT cooling age ● Exhumation[1]

**Figure_7.**

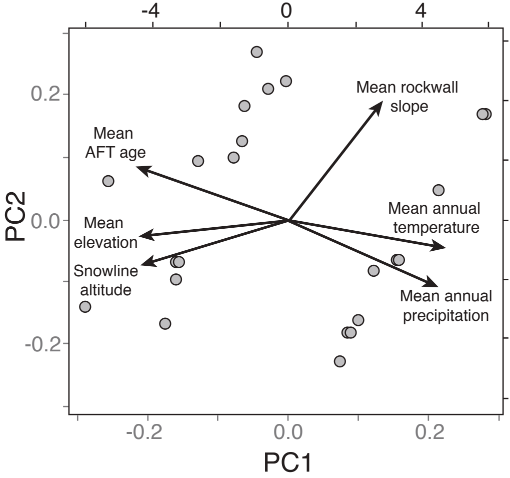
-4
0
4
0.2
0.0
-0.2
4
0
-4
PC2
PC1
-0.2
0.0
0.2
Mean rockwall slope
Mean AFT age
Mean elevation
Snowline altitude
Mean annual temperature
Mean annual precipitation

***Table 1.*** *Details of the investigated catchments*

| | Location[1] | | Climate | | | | Holocene glacial record | |
|---|---|---|---|---|---|---|---|---|
| **Catchment** | **Latitude** (°N) | **Longitude** (°E) | **Mean annual precip.[2, 3]** (mm/a) | **Mean annual temp.[4]** (°C) | **Min. catch. temp.[5]** (~°C) | **Mean rockwall temp.[5]** (~°C) | **Local glacial stages[6]** (ka) | **Regional glacial stages[7]** (ka) |
| **Ladakh** | | | | | | | | |
| Gopal | 33.9865 | 77.4571 | 87 (<500) | 5.6 | -13.0 | -10.6 | $M_{G1}$ (1.3±0.2 ka) | HH2 (~1.8−0.9 ka) |
| Stok | 33.9678 | 77.4698 | 87 (<500) | 5.6 | -11.6 | -9.7 | $M_{S1}$ (1.2±0.1 ka); $M_{S2}$ (0.6±0.2 ka) | HH1 (<1 ka); HH2 (~1.8−0.9 ka) |
| Amda | 33.6836 | 77.5925 | 87 (<500) | 5.6 | -12.3 | -9.8 | $M_{A1}$ (0.3±0.1 ka); $M_{A2C}$ (0.5±0.2 ka); $M_{A3}$ (1.6±0.3 ka) | HH1 (<1 ka); HH2 (~1.8−0.9 ka) |
| Karzok | 32.9681 | 78.1779 | 87 (<500) | 5.6 | -12.3 | -10.2 | $M_{G1}$ (2.1±0.3 ka); $M_{G2}$ (4.9±0.3 ka) | HH3 (~2.7−1.8 ka); HH5 (~6.9−4.3 ka) |
| Mentok | 32.9354 | 78.2124 | 87 (<500) | 5.6 | -13.7 | -11.6 | $M_{M1}$ (0.7±0.1 ka); $M_{M2}$ (1.0±0.1 ka) | HH1 (<1 ka); HH2 (~1.8−0.9 ka) |
| **Lahul-Spiti** | | | | | | | | |
| Urgos | 32.8970 | 76.7679 | 950 (500−1000) | 17.9 | -14.2 | -6.9 | - | - |
| Panchi | 32.7287 | 77.3009 | 950 (<500) | 17.9 | -12.1 | -5.8 | - | - |
| Shitidhar | 32.4197 | 77.1074 | 950 (<500) | 17.9 | -10.7 | -2.0 | - | - |
| Batal | 32.3640 | 77.6032 | 950 (<500) | 17.9 | -12.1 | -5.8 | - | - |
| Chhota Shigri | 32.2663 | 77.5288 | 950 (<500) | 17.9 | -12.8 | -5.5 | - | - |
| Hamtah | 32.2680 | 77.3572 | 950 (500−1000) | 17.9 | -12.8 | -5.8 | $M_{H1}$ (0.2±0.1 ka); $M_{H3}$ (10.4±0.3 ka) | HH1 (<1 ka); HH7 (~10.9−9.3 ka) |
| **Kullu** | | | | | | | | |
| Beas Kund | 32.3532 | 77.0890 | 1020 (500−1000) | 17.9 | -14.9 | -5.8 | - | - |

1: Catchment coordinates taken from glacier snout.

2: Mean annual precipitation. Rainfall data from local weather stations. Leh Meteorological Station (34.18°N, 77.58°E, 3500 m asl; CRUTEM4 1876–1990, Jones et al., 2012; Osborn and Jones, 2014): Gopal, Stok, Amda, Karzok and Mentok. Chhota Shigri weather station (32.28°N, 77.53°E, 3900 m asl; 1980−2005; Wagnon et al., 2007; Azam et al., 2014): Urgos, Panchi, Shitidhar, Batal, Chhota and Hamtah. Bhuntar Observatory (1969−2012; 31.8°N, 77.1°E, 1130 m asl; Azam et al., 2014): Beas Kund

3: (x) TRMM2B31 (1998−2009) annual rainfall data (Bookhagen and Burbank, 2010)

4:Temperature data from local weather stations. Leh Meteorological Station (34.18°N, 77.58°E, 3500 m asl; CRUTEM4 1876–1990, Jones et al., 2012; Osborn and Jones, 2014): Gopal, Stok, Amda, Karzok and Mentok. Chhota Shigri weather station (32.28°N, 77.53°E, 3900 m asl; 1980–2005; Wagnon et al., 2007; Azam et al., 2014): Urgos, Panchi, Shitidhar, Batal, Chhota Shigri, Hamtah and Beas Kund.

5: Temperatures estimated using local weather station data and an adiabatic lapse rate (ΔT/ΔZ) of 7°C/km Derbyshire et al., 1991; De Scally, 1997; Thayyen et al., 2005; Bashir and Rasul, 2010; Pratap et al., 2013; Kattel et al., 2013, 2015).

6: Local glacial stages from the northwestern end of the Himalayan-Tibetan orogen. Gopal: Saha et al. (2018); Stok: Orr et al. (2017), Saha et al. (2018); Amda: Orr et al. (2018), Saha et al. (2018); Karzok and Mentok: Hedrick et al. (2014), Saha et al., (2018); Hamtah: Saha et al. (2018).

7: Regional glacial stages from Saha et al. (2018). Holocene regional glacial stages for Ladakh include SWHTS 2A (12.2±0.8 ka), 1C (3.8±0.6 ka), 1B (1.7±0.2 ka) and 1A (0.4±0.1 ka) from Dortch et al. (2013). Regional stages for Lahul-Spiti and Kullu include MOHITS 2A (12.9±0.9 ka), 1K (11.4±0.7 ka), 1J (10.1±0.5 ka), 1I (9.1±0.3 ka), 1H (8.1±0.8 ka), 1G (7.7±0.6 ka), 1F (5.4±0.6 ka), 1E (3.5±0.4 ka), 1D (2.3±0.1 ka), 1C (1.5±0.2 ka), 1B (0.7±0.1 ka) and 1A (0.4±0.1 ka) from Murari et al. (2014).

***Table 2.*** *Catchment and glacier characteristics of the investigated catchments (uncertainties are expressed to 1σ)*

| Catchment | Catchment characteristics | | | | | | Glacier characteristics | | | | |
|---|---|---|---|---|---|---|---|---|---|---|---|
| | Area | Max. elevation | Relative relief[1] | Mean slope[2] | HI Index[3] | Rockwall area | Mean rockwall slope | Glacier area | Glacier aspect | Mean slope[2] | Modern ELA/SE[4] |
| | (~km$^2$) | (m asl) | (km) | (°) | | (~km$^2$) | (°) | (~km$^2$) | (°) | (°) | (m asl) |
| Gopal | 4.9 | 5920 | 1.0±0.1 | 27.3±12.6 | 0.4 | 4.2 | 33.9±11.8 | 0.7 | 22.5 | 13.4±6.9 | 5420±10 |
| Stok | 4.1 | 5930 | 0.7±0.1 | 26.6±12.4 | 0.5 | 3.1 | 30.8±11.8 | 1 | 45 | 14.4±6.7 | 5440±10 |
| Amda | 7 | 6000 | 0.8±0.2 | 26.9±15.7 | 0.5 | 5.3 | 35.2±15.5 | 1.7 | 90 | 12.4±6.6 | 5525±15 |
| Karzok | 3.9 | 5970 | 0.9±0.1 | 25.9±12.2 | 0.5 | 3.6 | 26.3±12.4 | 0.3 | 360 | 18.8±10.9 | 5550±10 |
| Mentok | 10.3 | 6200 | 0.9±0.2 | 21.1±13.6 | 0.4 | 7.6 | 35.5±13.0 | 2.7 | 22.5 | 13.8±7.8 | 5610±40 |
| Urgos | 30.3 | 6290 | 1.2±0.2 | 28.3±13.9 | 0.4 | 26.6 | 32.8±12.8 | 3.7 | 90 | 13.4±8.5 | 4830±25 |
| Panchi | 20.5 | 5945 | 1.3±0.3 | 29.5±14.0 | 0.4 | 16 | 34.8±12.1 | 4.5 | 360 | 14.7±8.7 | 4560±15 |
| Shitidhar | 22.2 | 5945 | 1.8±0.5 | 39.1±14.5 | 0.4 | 20.7 | 42.8±12.7 | 1.5 | 22.5 | 18.7±7.3 | 4050±10 |
| Batal | 13.9 | 5770 | 1.4±0.2 | 34.3±14.6 | 0.4 | 11.4 | 39.5±12.2 | 2.5 | 22.5 | 15.2±7.8 | 4700±15 |
| Chhota Shigri | 44.9 | 5600 | 1.3±0.3 | 29.4±15.8 | 0.5 | 31.6 | 36.5±14.8 | 13.3 | 360 | 16.2±9.2 | 4905±25 |
| Hamtah | 33.1 | 6155 | 1.2±0.3 | 32.2±14.9 | 0.4 | 28.3 | 39.2±12.2 | 4.8 | 360 | 10.6±6.0 | 4450±20 |
| Beas Kund | 17.6 | 5140 | 1.6±±0.3 | 35.3±16.3 | 0.4 | 16.6 | 47.2±11.9 | 1 | 360 | 13.1±8.7 | 3725±20 |

1: 3-km-radius relative relief

2: Slope calculated from 0.001km$^2$ catchment grid cells

3: Strahler (1952) Hypsometric Index (mean elevation- min elevation/relief)

4: Mean of equilibrium-line altitudes (ELA)/snowline elevation (SE) calculated using Area-altitude (AA), Area-accummulation ratio (AAR: 0.4,0.5,0.6) and Toe-headwall ratio (THAR: 0.4,0.5) methods from Benn et al. (2005) and Osmaston (2005).

***Table 3.*** *Medial moraine morphology and sediment descriptions*

| | D.C[1] | Medial moraine description | Supraglacial diamict description |
|---|---|---|---|
| Gopal | R | -Subdued moraine ridge; heterogeneous debris thickness (<5 mm−2 m). | -Sandy-boulder gravels with silt matrix; angular-sub angular clasts of leucogranite and granitic gneiss. |
| Stok | R | -Subdued moraine ridge; heterogeneous debris thickness (<5 mm−2 m); some soil development. | -Bouldery gravels; angular-sub angular clasts of leucogranite, granitic gneiss and schist. |
| Amda | R | -Moraine deposits along northern flank of Amda Kangri; heterogeneous debris thickness (<30 cm); some soil development and xerophytic shrubs. | -Sandy gravels with silt matrix containing interstitial ice; angular-sub angular clasts of leucogranite and schist. |
| Karzok | R | -Subdued moraine ridge (<10 m wide); heterogeneous debris thickness (<5 mm−10 m) | -Bouldery gravels with sandy matrix; very angular- sub angular clasts of leucogranite, gneiss and schist. |
| Mentok | R | -Moraine deposits at Mentok Kangri snout; heterogeneous debris thickness (<5 mm−3 m). | -Bouldery gravels with sandy matrix; very angular- sub angular clasts of leucogranite, gneiss and schist. |
| Urgos | C | -Distinct, steep relief medial moraine ridges; depressions and ice collapse features; heterogeneous debris thickness (<5 mm−5 m); discontinuous soil development, tundra vegetation and large boulders (>2−0.25 m) along and slightly offset from ridges. | -Sandy-boulder gravels with silt matrix containing interstitial ice; angular-sub angular clasts of leucogranite and granitic gneiss. |
| Panchi | C | -Steep relief medial moraine ridge; surface depressions; large ice cliff at glacier snout; restricted soil development. | -Sandy gravels with a silty-sand matrix; angular-sub rounded clasts of schist. |
| Shitidhar | P | -Subdued moraine deposits; heterogeneous debris thickness (<5 mm−2 m). | -Gravelly boulders with sandy matrix; very angular- angular clasts of leucogranite, gneiss and schist. |
| Batal | C | -Steep relief medial moraine ridge; ice cliffs; heterogeneous debris thickness (<5 mm−2 m); restricted soil development. | -Sandy-boulder gravels with silt matrix, angular-sub angular schistose clasts. |
| Chhota Shigri | C | -Distinct moraine ridges along length of ablation zone; heterogeneous debris thickness (<1cm−1 m); large boulders (>5 m) located along moraine ridge; soil development and tundra vegetation. | -Bouldery gravels with sandy-silt matrix, angular-sub rounded clasts of granite, granitic gneiss and schist. |
| Hamtah | C | -Distinct moraine ridges along length of ablation zone; heterogeneous debris thickness (<5mm−>5 m); soil development and tundra vegetation. | -Bouldery gravels with sandy-silt matrix, angular-sub rounded clasts of granitic gneiss and schist. |
| Beas Kund | P | -Steep relief medial moraine ridge, heterogeneous debris thickness (<5mm− 2 m); soil development restricted to moraine ridges | -Sandy-boulder gravels; angular- sub angular clasts of granite and gneiss. |

1: Debris cover: C- Complete debris coverage of the glacier ablation zone; P- Partial coverage (>30% of ablation zone surface); R- Restricted coverage (<30% of ablation zone surface)

***Table. 4.*** *Medial moraine sample details, $^{10}Be$ concentrations and inferred rockwall slope erosion rates for the investigated catchments*

| Sample | Catchment | Location | | | Cosmogenic $^{10}Be$ Data | | | | | Rockwall slope erosion rate | | | |
|---|---|---|---|---|---|---|---|---|---|---|---|---|---|
| | | Latitude (°N) | Longitude (°E) | Elevation (m asl) | Quartz mass (g) | $^{9}Be$ carrier mass,conc. (g, mg/g) | Native $^{9}Be$ (ug/g) | AMS $^{10}Be/^{9}Be$ ratio[1] ($10^{-15}$) | $^{10}Be$ concentration[2] ($10^4$ at/g) | $^{10}Be$ production rate (at/g/a) | Erosion rate (mm/a) | Snow corrected erosion rate[3] (mm/a) | Applicable time range (ka) |
| $G_{Gop1}$ | Gopal | 33.9865 | 77.4570 | 5294 | 23.3326 | 0.3496, 1.0082 | 0 | 208.2±7.0 | 20.9±0.7 | 105.3±13.6 | 0.3±0.04 | 0.3±0.04 | 2.0 |
| $G_{Stk1}$ | Stok | 33.9668 | 77.4684 | 5339 | 6.4552 | 0.3496, 1.0082 | 0 | 17.1±2.3 | 6.0±0.7 | 108.5±14.0 | 1.1±0.2 | 1.0±0.2 | 0.6 |
| $G_{Amd1}$ | Amda | 33.6833 | 77.5910 | 5340 | 25.8515 | 0.3490, 1.0255 | 0 | 120.0±5.2 | 10.8±0.3 | 107.1±13.9 | 0.5±0.1 | 0.6±0.1 | 1.2 |
| $G_{Amd2}$ | Amda | 33.6837 | 77.5909 | 5410 | 30.8093 | 0.3507, 1.0038 | 0 | 126.8±4.2 | 9.5±0.3 | 107.1±13.9 | 0.7±0.1 | 0.7±0.1 | 0.9 |
| $G_{Kar1}$ | Karzok | 32.9668 | 78.1775 | 5362 | 22.6878 | 0.3492, 1.0255 | 0 | 2022.4±34.3 | 213.0±3.5 | 105.9±13.7 | 0.03±0.004 | 0.03±0.004 | 20.1 |
| $G_{Kar2}$ | Karzok | 32.9665 | 78.1776 | 5367 | 13.2533 | 0.3506, 1.0038 | 0 | 1205.0±18.8 | 214.0±3.2 | 105.9±13.7 | 0.03±0.004 | 0.03±0.004 | 20.2 |
| $G_{Kar3}$ | Karzok | 32.9663 | 78.1776 | 5371 | 27.3612 | 0.3507. 1.0038 | 0.01 | 3027.6±146.2 | 260.0±12.5 | 105.9±13.7 | 0.02±0.004 | 0.02±0.004 | 24.6 |
| $G_{Men1}$ | Mentok | 32.9332 | 78.2107 | 5506 | 29.3919 | 0.3497, 1.0255 | 0 | 406.4±16.3 | 32.9±1.2 | 107.5±13.9 | 0.2±0.03 | 0.2±0.03 | 3.2 |
| $G_{Urg1}$ | Urgos | 32.8990 | 76.7646 | 4420 | 17.6703 | 0.3505, 1.0038 | 0.01 | 16.3±2.4 | 1.7±0.2 | 90.2±11.7 | 3.2±0.5 | 3.0±0.5 | 0.2 |
| $G_{Urg2}$ | Urgos | 32.8999 | 76.7635 | 4434 | 20.0819 | 0.3491, 1.0038 | 0.01 | 9.5±1.0 | 0.7±0.02 | 90.2±11.7 | 7.6±1.0 | 7.5±1.0 | 0.1 |
| $G_{Pan1}$ | Panchi | 32.7244 | 77.3020 | 4349 | 0.3987 | 0.3508, 1.0082 | 0 | 3.7±1.2 | 19.3±4.5 | 77.9±10.1 | 0.2±0.1 | 0.2±0.1 | 2.5 |
| $G_{Sht1}$ | Shitidhar | 32.4159 | 77.1049 | 3568 | 4.6600 | 0.3494, 1.0082 | 0 | 6.8±1.2 | 3.2±0.4 | 60.2±7.8 | 1.1±0.2 | 1.1±0.2 | 0.5 |
| $G_{Bat1}$ | Batal | 32.3628 | 77.6012 | 4310 | 11.3517 | 0.3505, 1.0082 | 0 | 147.4±5.3 | 30.6±1.0 | 81.0±10.5 | 0.2±0.02 | 0.2±0.02 | 3.8 |
| $G_{Bat2}$ | Batal | 32.3609 | 77.5981 | 4368 | 6.3124 | 0.3495, 1.0082 | 0 | 9.8±1.3 | 3.5±0.3 | 81.0±10.5 | 1.4±0.2 | 1.3±0.2 | 0.4 |
| $G_{Cht1}$ | Chhota Shigri | 32.2639 | 77.5283 | 4273 | 27.0872 | 0.3488, 1.0255 | 7.9 | 39.9±5.3 | 3.2±0.3 | 82.6±10.7 | 1.5±0.3 | 1.5±0.3 | 0.4 |
| $G_{Cht2}$ | Chhota Shigri | 32.2635 | 77.5283 | 4281 | 26.4000 | 0.3496, 1.0038 | 4.7 | 46.1±4.5 | 3.9±0.3 | 82.6±10.7 | 1.3±0.2 | 1.3±0.2 | 0.5 |
| $G_{Cht3}$ | Chhota Shigri | 32.2629 | 77.5285 | 4292 | 27.4440 | 0.3501, 1.0822 | 0 | 49.0±16.5 | 4.2±1.3 | 82.6±10.7 | 1.2±0.4 | 1.1±0.4 | 0.5 |
| $G_{Cht4}$ | Chhota Shigri | 32.2621 | 77.5287 | 4316 | 18.7804 | 0.3487, 1.0255 | 40.5 | 12.0±1.5 | 1.1±0.004 | 82.6±10.7 | 4.4±0.6 | 4.2±0.6 | 0.1 |
| $G_{Cht5}$ | Chhota Shigri | 32.2611 | 77.5282 | 4336 | 29.3671 | 0.3509, 1.0038 | 0 | 14.0±1.3 | 1.0±0.05 | 82.6±10.7 | 5.1±0.7 | 4.8±0.7 | 0.1 |
| $G_{Ham1}$ | Hamtah | 32.2643 | 77.3583 | 4085 | 27.9648 | 0.3493, 1.0255 | 0.01 | 17.9±1.5 | 1.3±0.01 | 72.0±9.3 | 3.4±0.4 | 3.2±0.4 | 0.2 |
| $G_{Ham2}$ | Hamtah | 32.2640 | 77.3579 | 4083 | 26.2989 | 0.3492, 1.0038 | 0 | 24.5±3.2 | 2.0±0.2 | 72.0±9.3 | 2.1±0.4 | 2±0.4 | 0.3 |
| $G_{Ham3}$ | Hamtah | 32.2635 | 77.3585 | 4091 | 25.0875 | 0.3511, 1.0255 | 0.05 | 15.5±3.4 | 1.2±0.2 | 72.0±9.3 | 3.7±0.7 | 3.5±0.7 | 0.2 |
| $G_{Ham4}$ | Hamtah | 32.2626 | 77.3582 | 4095 | 29.8146 | 0.3492, 1.0038 | 0 | 11.8±2.2 | 0.8±0.1 | 72.0±9.3 | 5.5±1.1 | 5.2±1.1 | 0.1 |
| $G_{Bea1}$ | Beas Kund | 32.3543 | 77.0858 | 3604 | 26.9295 | 0.3496, 1.0038 | 0.005 | 6.8±0.9 | 0.6±0.05 | 52.6±6.8 | 5.7±0.9 | 5.4±0.9 | 0.1 |
| $G_{Bea2}$ | Beas Kund | 32.3536 | 77.0863 | 3594 | 25.8173 | 0.3499, 1.0038 | 0.015 | 9.2±1.5 | 0.8±0.1 | 52.6±6.8 | 4.0±0.7 | 3.8±0.7 | 0.2 |
| $G_{Bea3}$ | Beas Kund | 32.3534 | 77.0864 | 3579 | 24.7578 | 0.3510, 1.0038 | 0.01 | 5.3±0.8 | 0.5±0.04 | 52.6±6.8 | 6.8±1.0 | 6.5±1.0 | 0.1 |

1: $^{10}Be/^{9}Be$ ratios are corrected for background $^{10}Be$ detected in full procedural blanks($G_{Amd}$1, $G_{Kar1}$, $G_{Men1}$; $G_{Cht2,4}$, $G_{Ham1}$, $G_{Kar1}$, $G_{Men1}$: 3.14±1.43x$10^{-15}$; $G_{Cht3}$: 3.14±2.47x$10^{-15}$; $G_{Amd2}$, $G_{Kar2}$, $G_{Cht2,5}$, $G_{Ham2,4}$: 1.55±0.64x$10^{-15}$; $G_{Bea1-3}$: 4.15±0.39x$10^{-15}$; $G_{Kar3}$, $G_{Urg1,2}$: 3.41±1.08x$10^{-15}$; $G^{Gop1}$, $G^{Stk1}$, $G^{Pan1}$, $G^{Sht1}$, $G^{Bat1,2}$: 4.15±3.9x$10^{-16}$.

2: Accummulation of $^{10}Be$ during burial, englacial transport and exhumation (0.01x$10^4$-0.03x$10^4$ at/g) is calculated using methods detailed in Ward and Anderson (2011; see Supplementary Item 2). Accummulation is subtracted from the total concentration.

3: Erosion rates of corrected for shielding via snow (see Methods section).

***Table 5.*** *Pearson's Correlation Coefficient values (p) between $^{10}$Be rockwall slope erosion rates and catchment matrices.*

| | | | Rockwall slope erosion rate |
|---|---|---|---|
| | | Max. grain size (2) | 0.7 |
| Catchment | charact. | Catchment area (>10) | 0.0003 |
| | | Rockwall area (>10) | 0.002 |
| | | Peak elevation (>10) | 0.8 |
| | | Mean elevation (>10) | 0.0001 |
| | | Snowline elevation (>10) | 0.00006 |
| | | Catchment relief (>10) | 0.2 |
| | | Catchment slope (>10) | 0.006 |
| | | Rockwall slope (>10) | 0.00002 |
| Glacier | charact. | Glacier area (>10) | 0.02 |
| | | Glacier aspect (>10) | 0.5 |
| | | Mean glacier slope (>10) | 0.02 |
| | | Glacier velocity (5) | 0.8 |
| Climatic | conditions | Mean annual precip.[1] (4) | 0.0007 |
| | | Mean annual temp.[2] (3) | 0.000004 |
| | | Min. catchment temp.[3] (3) | 0.5 |
| | | Mean rockwall temp.[3] (>10) | 0.1 |
| | | Lithology (2) | 0.8 |
| | | Mean AFT age[4] (8) | 0.0000030 |

( ): Class size

1: Mean annual precipitation (see Table 1).

2: Temperature data from local weather stations (Table 1).

3: Temperatures estimated using local weather station data and an adiabatic lapse rate (ΔT/ΔZ) of 7°C/km (Derbyshire et al., 1991; De Scally, 1997; Thayyen et al., 2005; Siddiqui and Maruthi, 2007; Bashir and Rasul, 2010; Pratap et al., 2013; Kattel et al., 2013, 2015).

4: Mean of AFT ages from Sorkhabi et al. (1996), Searle et al. (1999), Jain et al. (2000), Schlup et al. (2003, 2011), Thiede et al. (2004, 2005, 2006, 2008, 2009), Vannay et al. (2004), Kristein et al. (2006, 2009), Walia et al. (2008) and van der Beek et al. (2009).